The Astrophysical Journal, 709:884–911, 2010 February 1 doi:10.1088/0004-637X/709/2/884


# THE ROLE OF STARBURST–ACTIVE GALACTIC NUCLEUS COMPOSITES IN LUMINOUS INFRARED GALAXY MERGERS: INSIGHTS FROM THE NEW OPTICAL CLASSIFICATION SCHEME

T.-T. Yuan, L. J. Kewley, and D. B. Sanders
Institute for Astronomy, University of Hawaii, 2680 Woodlawn Drive, Honolulu, HI 96822, USA; yuantt@ifa.hawaii.edu, kewley@ifa.hawaii.edu, sanders@ifa.hawaii.edu
*Received 2007 December 18; accepted 2009 November 23; published 2010 January 8*

## ABSTRACT

We investigate the fraction of starbursts, starburst–active galactic nucleus (AGN) composites, Seyferts, and low-ionization narrow emission-line region galaxies (LINERs) as a function of infrared luminosity ($L_{\rm IR}$) and merger progress for ∼500 infrared (IR)-selected galaxies. Using the new optical classifications afforded by the extremely large data set of the Sloan Digital Sky Survey, we find that the fraction of LINERs in IR-selected samples is rare (<5%) compared with other spectral types. The lack of strong IR emission in LINERs is consistent with recent optical studies suggesting that LINERs contain AGN with lower accretion rates than in Seyfert galaxies. Most previously classified IR-luminous LINERs are classified as starburst–AGN composite galaxies in the new scheme. Starburst–AGN composites appear to "bridge" the spectral evolution from starburst to AGN in ULIRGs. The relative strength of the AGN versus starburst activity shows a significant increase at high IR luminosity. In ULIRGs ($L_{\rm IR} > 10^{12}\ L_{\odot}$), starburst–AGN composite galaxies dominate at early–intermediate stages of the merger, and AGN galaxies dominate during the final merger stages. Our results are consistent with models for IR-luminous galaxies where mergers of gas-rich spirals fuel both starburst and AGN, and where the AGN becomes increasingly dominant during the final merger stages of the most luminous IR objects.

*Key words:* galaxies: active – galaxies: evolution – galaxies: interactions – galaxies: starburst – infrared: galaxies

*Online-only material:* color figures

## 1. INTRODUCTION

Luminous infrared galaxies (LIRGs; $L_{\rm IR} > 10^{11}\ L_{\odot}$[1]) were first discovered in small numbers ∼4 decades ago (Low & Kleinmann 1968; Kleinmann & Low 1970a, 1970b; Becklin et al. 1971; Becklin & Neugebauer 1972; Rieke & Low 1972). The importance of these objects to galaxy evolution was made more clear following the first all-sky survey carried out by the *Infrared Astronomical Satellite* (*IRAS*; Neugebauer et al. 1984). Soifer et al. (1987) found that the space density of infrared (IR)-selected LIRGs in the local universe ($z < 0.1$) rivaled that of the most powerful optically selected starburst and Seyfert galaxies at similar bolometric luminosity, and that the most luminous objects—ultraluminous infrared galaxies (ULIRGs; $L_{\rm IR} > 10^{12}\ L_{\odot}$)—had similar space densities and bolometric luminosities as optically selected quasi-stellar objects (QSOs).

There have been numerous studies related to the origin and evolution of U/LIRGs,[2] and most now seem to agree that strong interactions and mergers of gas-rich galaxies are the trigger for the majority of the more luminous LIRGs (see the review by Sanders & Mirabel 1996). The merger fraction increases with IR luminosity and approaches 100% for samples of ULIRGs (e.g., Sanders et al. 1988a; Kim 1995; Clements et al. 1996; Farrah et al. 2001). In the complete sample of *IRAS* 1 Jy ULIRGs by Kim (1995), 117 out of 118 galaxies show strong signs of tidal interaction (Veilleux et al. 2002).

There is less consensus on the nature of the power source of U/LIRGs. It is clear that the IR luminosity in U/LIRGs can derive from dust reprocessing of either extreme starburst activity, active galactic nucleus (AGN), or a combination of the two. Studies of moderate to large samples of U/LIRGs (e.g., Kim 1995; Veilleux et al. 1995; Goldader et al. 1995; Genzel et al. 1998) indicate that the dominant power source in lower luminosity LIRGs is an extended starburst, and that an AGN often makes an increasing contribution to the bolometric luminosity in the more luminous sources with obvious energetic point-like nuclei. However, different studies of the same objects disagree on the relative contributions of starburst and AGN activity to the bolometric luminosity, in particular for the ULIRGs where the dominant energy source powering their extremely luminous and compact nuclear cores continues to be the subject of intense debate (compared to Joseph 1999; Sanders 1999). Although numerous studies at various wavelengths continue to be carried out to determine the energy source of ULIRGs (e.g., Tran et al. 2001; Farrah et al. 2003, 2007; Lípari et al. 2003; Ptak et al. 2003; Imanishi et al. 2007), determining the relative contribution of starbursts and AGN within individual galaxies is still difficult.

One of the commonly proposed merger scenarios for ULIRGs (e.g., Sanders et al. 1988a; Kim et al. 1995; Farrah et al. 2001; Lípari et al. 2003; Dasyra et al. 2006) is based on the Toomre & Toomre (1972) sequence in which two galaxies lose their mutual orbital energy and angular momentum to tidal features and/or an extended dark halo and coalesce into a single galaxy. Tidal interactions and associated shocks are thought to trigger star formation (e.g., Bushouse 1987; Kennicutt et al. 1987; Liu & Kennicutt 1995; Barnes 2004) which heats the surrounding dust, producing strong far-infrared (FIR) radiation. The FIR radiation rises to an ultraluminous IR stage powered by starbursts and/or dust-shrouded AGN. As starburst activity subsides, the merger finally evolves into an optically bright QSO. In this scenario, ULIRGs plausibly represent a dust-shrouded transition stage

[1] $L_{\rm IR} \equiv L(8\text{–}1000\ \mu\text{m})$; see Sanders & Mirabel (1996).

[2] Previous studies of the properties of IR galaxies versus $\log(L_{\rm IR}/L_{\odot})$ often divide the galaxy samples into decade luminosity bins and use the terms moderate, luminous, ultraluminous, and hyperluminous to refer to the decade ranges 10–10.99, 11–11.99, 12–12.99, and 13–13.99, respectively. We follow this convention here, and use U/LIRGs when we wish to refer to all galaxies with $\log(L_{\rm IR}/L_{\odot}) = 11\text{–}12.99$.

that leads to the formation of optical QSOs (e.g., Sanders et al. 1988b; Dasyra et al. 2006; Kawakatu et al. 2006; Zauderer et al. 2007).

A key element in testing the above scenario is to clarify the power source behind the strong IR emission, and the relationship between this power source and the evolutionary stage of the interaction. Comprehensive studies on large IR-selected samples are crucial to this analysis. Notable examples of such samples are the *IRAS* Bright Galaxy Survey (BGS; Veilleux et al. 1995), the *IRAS* 1 Jy ULIRGs sample (1 Jy ULIRGs; Kim 1995; Kim & Sanders 1998; Veilleux et al. 2002), and the Southern Warm Infrared Galaxy sample (SW01; Kewley et al. 2001b).

Most previous studies use standard optical spectral diagnostic diagrams to classify the dominant power source in emission-line galaxies (Baldwin et al. 1981; Veilleux & Osterbrock 1987). These diagrams are based on four optical emission-line ratios that are sensitive to the hardness of the ionizing radiation field. More recently, the Sloan Digital Sky Survey (SDSS) has revolutionized these classification schemes by revealing clearly formed branches of star-forming galaxies, Seyferts, and low-ionization narrow emission-line region galaxies (LINERs) on the diagnostic diagrams, for the first time (Kewley et al. 2006). Kewley et al. show that many galaxies previously classified as LINERs lie along a well-defined mixing branch from star-forming galaxies to Seyfert galaxies.

In light of this new classification scheme, we investigate the new spectral classification of IR galaxies as a function of IR luminosity and merger progress. We describe our sample selection and derived quantities in Section 2. The results are presented in Section 3. We discuss the results in Section 4 and summarize in Section 5. For convenience of comparison with the old 1 Jy ULIRG analysis by Veilleux et al. (1999, 2002), we adopt a Hubble constant of $H_0 = 75$ km s$^{-1}$ Mpc$^{-1}$, and $\Omega_m = 0.27$, $\Omega_\Lambda = 0.73$ throughout the paper.

## 2. SAMPLE SELECTION AND DERIVED QUANTITIES

### 2.1. Sample Selection

We use three local samples of IR-selected galaxies: the 118 ULIRGs from the *IRAS* 1 Jy sample of ULIRGs (Kim & Sanders 1998; hereafter the 1 Jy ULIRGs sample), 104 of the highest luminosity objects from the *IRAS* Bright Galaxy Survey (hereafter the BGS sample), and the complete sample of 285 galaxies in the Southern Warm Infrared Galaxies sample (Kewley et al. 2001b; hereafter the SW01 sample).

The complete 1 Jy sample was compiled by Kim (1995) and is described in detail in Kim & Sanders (1998). The 1 Jy sample was selected from the *IRAS* Faint Source Catalog (FSC) with flux $F(60\ \mu\mathrm{m}) > 1$ Jy at high Galactic latitude $|b| > 30^\circ$, and declination $\delta > -40^\circ$. The sample contains 118 objects with redshift $z = 0.02$–$0.27$ and $\log(L_{\rm IR}/L_\odot) = 12.00$–$12.90$. Veilleux et al. (1999) published optical spectra for 108 of these objects at a resolution of 8.3 Å. Their nuclear spectra were extracted using a window corresponding to a physical diameter of 4 kpc (for the three objects with $z > 0.2$: IRAS 00397−1312, IRAS 12032+1707, and IRAS 23499+2434, a diameter of 8 kpc was used). Typical uncertainties for the emission-line ratios are 5%–10%. A $R$- and $K'$-band image atlas for the 1 Jy sample is given in Kim et al. (2002) and the analysis of the morphological properties was carried out by Veilleux et al. (2002).

We also include 104 lower luminosity objects from the *IRAS* BGS (Sanders et al. 1995; Veilleux et al. 1995; Soifer et al. 1986, 1987, 1989). The BGS represents all extragalactic sources brighter than 5.24 Jy at 60 $\mu$m, $|b| > 5^\circ$. Kim et al. (1995) provide optical spectra for 114 of these objects at a resolution of 8–10 Å. A constant linear aperture of 2 kpc was used to extract the nuclear spectra. The redshift range is $z = 0.0027$–$0.09$ with a median of 0.02. Among the original 114 BGS objects in Kim et al. (1995), a total of 10/114 are ULIRGs, with eight of the ULIRGs also included in the 1 Jy sample. We only use the 104 LIRGs ($\log(L_{\rm IR}/L_\odot) < 12.0$) in the BGS sample. The main role of the BGS sample in this study is to supplement the 1 Jy ULIRG sample with lower luminosity objects, and to help create a larger non-ULIRGs sample in Section 3.4. The final $L_{\rm IR}$ range is $\log(L_{\rm IR}/L_\odot) = 10.5$–$13.0$ for the 1 Jy ULIRG and BGS samples combined.

The SW01 sample was selected by Kewley et al. (2001b) from the catalog of Strauss et al. (1992). It consists of 285 *IRAS* galaxies with $F(60\ \mu\mathrm{m}) > 2.5$ Jy at $|b| > 15^\circ$, $\delta < 0^\circ$. Kewley et al. (2001b) applied the "warm" color criteria ($F_{60}/F_{25} < 8$) to ensure that the sample contains a high fraction of AGN. SW01 has a wide coverage in IR luminosity, and is dominated by LIRGs: among the total 285 galaxies, 277 galaxies have $\log(L_{\rm IR}/L_\odot) = 8.0$–$11.99$ and 8 are ULIRGs. Kewley et al. (2001b) took high-resolution spectra (30 km s$^{-1}$ at H$\alpha$) for 235 objects in the SW01 sample (the emission-line intensity measurements are accurate to within 30%). The SW01 redshift limit is $z < 0.027$ for IR luminosities $\log(L_{\rm IR}/L_\odot) < 11.0$ and $z < 0.067$ for $\log(L_{\rm IR}/L_\odot) > 11.0$. Their nuclear spectra were extracted using an aperture corresponding to 1 kpc at the redshift of each galaxy.

For the BGS and SW01 samples, we use optical images from the Digitized Sky Survey (DSS) and $K_s$-band images from Two Micron All Sky Survey (2MASS). We use the $K_s$-band images to obtain the projected nuclear separation for the interacting galaxies in our samples and use the $R$ band and other available optical band images for identification of tidal debris.

### 2.2. Optical Classification

The classification of the dominant energy source in emission-line galaxies using optical emission-line ratios was first proposed by Baldwin et al. (1981, hereafter BPT). BPT proposed the use of the [O III]λ5007/H$\beta$, [N II] λ6583/H$\alpha$, and [O I] λ6300/H$\alpha$ line ratios for spectral classification, taking advantage of the sensitivity of these line ratios to the hardness of the ionizing radiation field. Kennicutt & Keel (1984) and Keel (1983) extended the initial set of classification ratios to include the [S II]λλ6716, 6731/H$\alpha$ line ratio which is also sensitive to the hardness of the ionizing radiation field and observable in the optical regime. To improve the optical classification, Osterbrock & de Robertis (1985) and Veilleux & Osterbrock (1987, hereafter VO87) derived the first semi-empirical classification lines to be used with the standard optical diagnostic diagrams. Because of the pioneering work of Baldwin et al. (1981) and Veilleux & Osterbrock (1987), the "standard optical diagnostic diagrams" based on the [O III]/H$\beta$, [N II]/H$\alpha$, [S II]/H$\alpha$, and [O I]/H$\alpha$ line ratios are commonly known as BPT or VO87 diagrams.

Large samples or active galaxies reveal a tight abundance sequence for star-forming galaxies and an AGN sequence that begins at the metal-rich end of the star-forming abundance sequence and extends toward the upper right corner of the diagnostic diagrams (i.e., toward large [O III]/H$\beta$, [N II]/H$\alpha$, [S II]/H$\alpha$, and [O I]/H$\alpha$).

The first purely theoretical classification scheme was developed by Kewley et al. (2001a, hereafter Ke01). Ke01 used a

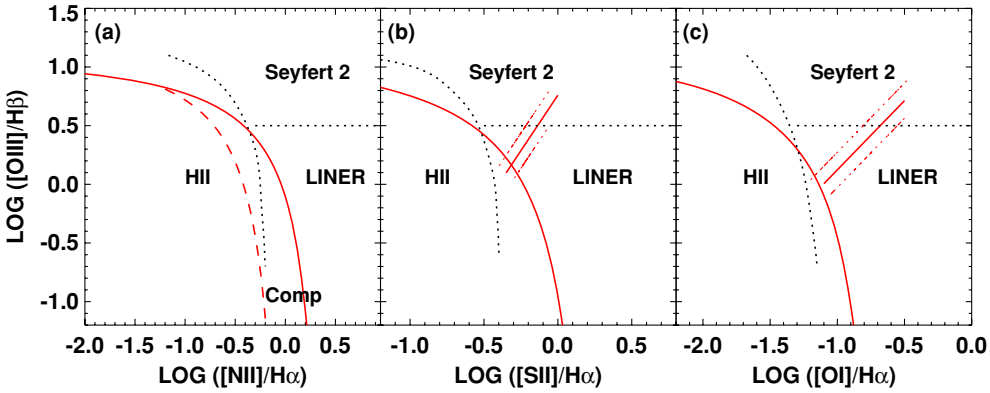


**Figure 1.** Standard optical diagnostic diagrams showing the previous optical classification scheme by Veilleux & Osterbrock (1987) (black dotted lines) and the new classification scheme by Kewley et al. (2006). Star-forming galaxies form a tight abundance sequence on these diagnostic diagrams. The AGN branch begins at the metal-rich end of the star-forming galaxy sequence and extends toward the upper right corner of these diagrams. Red solid curves are the theoretical "maximum starburst line" derived by Kewley et al. (2001a) as an upper limit for star-forming galaxies (see more descriptions in Section 2.2); the red dashed curve on the [N II] diagram is the Kauffmann et al. (2003) semi-empirical lower boundary for the star-forming galaxies; the red lines (with the empirical error ±0.1 dex lines) on [S II] and [O I] diagrams are the empirical boundary lines between Seyfert 2 galaxies and LINERs. See Section 2.2 for more details. The Kewley et al. (Ke06) scheme substantially changes the LINER boundaries, and includes a class for starburst–AGN composites (labeled Comp). Note that in the [N II] λ6583/Hα vs. [O III]/Hβ diagram (panel a), the VO87 scheme distinguishes between Seyfert 2 galaxies and LINERs, while the Ke06 classification scheme does not.

(A color version of this figure is available in the online journal.)

combination of modern stellar population synthesis, photoionization, and shock models to derive a "maximum starburst line" on the BPT diagrams. Galaxies that lie above this line cannot be explained by any combination of starburst models and require a dominant (>50%) contribution from an AGN. Galaxies that lie below the Ke01 line may include a non-dominant (i.e., <50%) contribution from an AGN.

To obtain a more stringent sample of star-forming galaxies, Kauffmann et al. (2003, hereafter Kau03) shifted the Ke01 line to form a semi-empirical upper boundary for the star-forming branch observed with the SDSS. The Kau03 line retains the shape of the Ke01 theoretical models, with a shift to enable the classification of pure star-forming galaxies (i.e., 100% star formation dominated). The combination of the Ke01 and Kau03 lines serves to separate pure star-forming galaxies, galaxies that are likely to contain both star formation and AGN activity (composite galaxies), and galaxies that are dominated by their AGN.

Kewley et al. (2006, hereafter Ke06) showed that AGN sequence forms two clear branches on the [S II]/Hα and [O I]/Hα diagnostic diagrams. These two branches were revealed with the large number of SDSS galaxies (∼45,000); these branches were not observed with the smaller sample sizes (∼200) that were used in previous studies (e.g., VO87 and Ke01). Ke06 derived empirical boundary lines between Seyfert 2s and LINERs on the [S II]/Hα and [O I]/Hα diagrams based on the observed local minimum between the Seyfert and LINER branches. Seyfert and LINER galaxies defined in this way have significant differences in their host properties; LINERs are older, more massive, less dusty, and less concentrated than Seyfert galaxies. However, at fixed accretion rate, these differences disappear. LINERs and Seyferts form a continuous sequence in Eddington rate from low to high Eddington rates, respectively. Ke06 conclude that LINERs are AGNs and that the dichotomy between Seyferts and LINERs is analogous to the high and low states observed in X-ray binary systems.

As in X-ray binaries, LINERs have a harder ionizing radiation field and lower ionization parameter than Seyfert galaxies. These characteristics make the [S II]/Hα and [O I]/Hα diagrams ideal for separating Seyferts and LINERs. The [S II] and [O I] emission lines are produced in the partially ionized zone at the edge of the nebula; this zone is large and extended for hard radiation fields. Power-law AGN models from Groves et al. (2004) indicate that models with a hard radiation field and low-ionization parameter are separated in the [S II]/Hα and [O I]/Hα diagrams; these ratios change by ∼0.7 dex as the power-law index is changed from −1.2 to −2.0.

Note that the [N II]/Hα ratio diagram cannot be used to separate Seyferts and LINERs. The [N II]/Hα ratio is only weakly dependent on the hardness of the radiation field; log([N II]/Hα) only changes by 0.2 dex as the power-law index is varied from −1.2 to −2.0 (Groves et al. 2004). The [N II]/Hα ratio is much more strongly dependent on the metallicity of the nebular gas. Metallicity differences among AGN host galaxies plus the weak dependence on hardness renders the [N II]/Hα diagram insensitive to the major differences between Seyfert and LINERs seen in the [S II]/Hα and [O I]/Hα diagrams.

Ke06 estimated empirical errors (±0.1 dex) for the Seyfert–LINER boundary by considering the positions of galaxies that remain Seyfert 2 or that remain LINER in both the [S II]/Hα and [O I]/Hα diagrams. The class of galaxies that lie within ±0.1 dex of the Seyfert 2/LINER line is uncertain.

In Figure 1, we show the difference between the previous VO87 classification scheme (black dotted lines) and the new Ke06 classification scheme (red solid and dashed lines). Galaxies that were previously classified as LINERs may be either (a) true LINERs, (b) composite H II–AGN galaxies, or (c) Seyfert 2 galaxies, or (d) high-metallicity star-forming galaxies, according to the new classification scheme. A substantial fraction (∼ 1/3) of ULIRGs and LIRGs have been previously classified as LINERs using the VO87 method (Veilleux et al. 1995, 1999). Therefore, the application of the Ke06 classification scheme may reveal new insight into the power source behind IR-selected galaxies previously classified as LINERs.

In addition to the major change in LINER classification, the Ke06 scheme includes starburst–AGN composite galaxies as a separate class of objects. The [N II]/Hα versus [O III]/Hβ diagram is used to classify composite galaxies. (Composite galaxies lie between the red dashed and solid lines in Figure 1(a).) The [N II]/Hα ratio is more sensitive to the presence of a low-level AGN than the [S II]/Hα, and [O I]/Hα line ratios because the

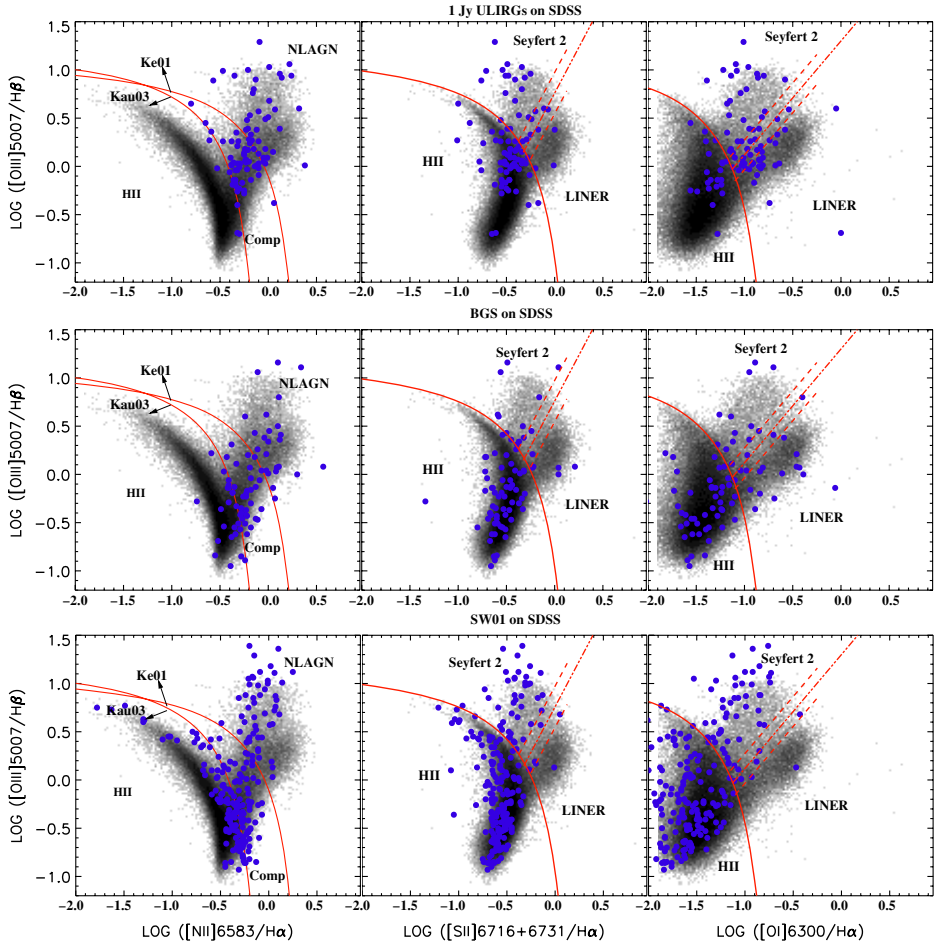


**Figure 2.** Samples (blue filled circle) used in this work are shown on the BPT diagrams, over-plotted are the SDSS galaxies (black dots) from Kewley et al. (2006). The curves and lines have the same meaning as in Figure 1, i.e., upper red curves on all three BPT diagrams are the theoretical "maximum starburst line;" the lower red curve on the [N II] diagram is the Kauffmann et al. (2003) semi-empirical lower boundary for star-forming galaxies, and the red lines (with the empirical error ±0.1 dex lines) in [S II] and [O I] diagrams are the empirical boundary lines between Seyferts and LINERs. See the text in Section 2.2 for more details. From top to bottom, the samples are: 1 Jy ULIRGs, BGS, and SW01. The red lines are the new classification scheme Kewley et al. (2006) used to separate starburst (H II-region) galaxies, starburst–AGN composite galaxies, Seyfert 2, and LINERs. In the leftmost panels, NLAGN ≡ narrow emission-line AGN (Seyfert 2 plus LINERs); Comp ≡ starburst–AGN composites.

(A color version of this figure is available in the online journal.)

[N II]/H$\alpha$ ratio is a linear function of nebular metallicity until high metallicities where the [N II]/H$\alpha$ reaches a plateau at $\log([\mathrm{N\,II}]/\mathrm{H}\alpha) \sim -0.5$ (Kewley & Dopita 2002; Denicoló et al. 2002; Pettini & Pagel 2004). At this plateau, any AGN contribution shifts the [N II]/H$\alpha$ ratio above $\log([\mathrm{N\,II}]/\mathrm{H}\alpha) > -0.5$. An AGN contribution to low-metallicity galaxies is extremely rare (Groves et al. 2006).

We apply the new Ke06 classification scheme to our three samples to discriminate between star-forming galaxies (or starburst/H II-region galaxies), Seyfert 2, LINERs, and starburst–AGN composites. In Figure 2, our three samples are shown in comparison with the SDSS galaxies used in Kewley et al. (2006) on the BPT diagrams with the new classification boundaries. The Ke06 classification scheme that we use in this work is as follows.

1. Star-forming galaxies lie below and to the left of Kau03 line on the [N II]/H$\alpha$ diagram (e.g., Figure 2, left column, the lower red solid line), and below and to the left of Ke01 theoretical lines in the [S II]/H$\alpha$ and [O I]/H$\alpha$ diagrams (e.g., Figure 2, middle and right columns, the red solid lines).
2. Starburst–AGN composites lie above the Kau03 line but below and to the left of the Ke01 theoretical line in the [N II]/H$\alpha$ diagram (Figure 2, left column).
3. Seyfert 2 galaxies lie above the Ke01 theoretical lines on all three BPT diagrams and also above the Seyfert–LINER boundary lines in the [S II]/H$\alpha$ and [O I]/H$\alpha$ diagrams (e.g., Figure 2, middle and right columns).
4. LINERs lie above the Ke01 theoretical lines on all three BPT diagrams and below the Seyfert–LINERs boundary lines on the [S II]/H$\alpha$ and [O I]/H$\alpha$ diagrams.
5. Ambiguous galaxies are those that are classified as one type of object in one or two diagrams and are classified as another type in the remaining diagram(s).
6. Seyfert 1 galaxies are not included on the BPT diagrams and are considered separately. They are characterized by their broad Balmer emission lines—usually H$\alpha$(FWHM) $> 5 \times 10^3$ km s$^{-1}$. Thus, galaxies classified as Seyfert 1 in previous studies remain classed as Seyfert 1 in our study.

The most stringent method for the classification of galaxies using this scheme is to use all three diagnostic diagrams. We refer to the use of all three diagnostic diagrams hereafter as

the "3-of-3" criterion. The use of all three diagnostic diagrams allows for ambiguous galaxies to be classified separately. For data sets with a significant fraction of unmeasurable or uncertain [S II]/H$\alpha$ or [O I]/H$\alpha$ ratios, an alternative "2-of-3" criterion is often applied. This method applies the majority class, i.e., if two out of three diagnostic diagrams give one class, but the third diagram gives a different class or is unavailable, the consistent class of the remaining two diagnostic diagrams is assumed. There is no ambiguous class if the 2-of-3 criterion is applied. Most previous studies on the optical classification of IR galaxies apply the 2-of-3 criterion (Veilleux et al. 1995, 1999, 2002). The [S II]/H$\alpha$ classifications are uncertain for a substantial portion ($\sim$16%–17%) of the BGS and 1 Jy ULIRG samples (i.e., the [S II]/H$\alpha$ class lies within the 0.1 dex uncertainty line defined in Ke01). For comparison with previous work and to avoid contamination by uncertain [S II]/H$\alpha$ classifications, we apply the "2-of-3" criterion to our samples. We discuss our results in the context of the 3-of-3 criterion in Appendix B.

In the 1 Jy ULIRG sample, the 2-of-3 classification scheme yields eight (7.8%) star-forming galaxies, 46 (44.7%) starburst–AGN composites, 35 (33.9%) Seyfert 2, 10 (9.7%) Seyfert 1, and four (3.9%) LINERs. These classes include the nine galaxies in the 1 Jy sample with double nuclei that have spectra taken for both nuclei. Of these double-nuclei galaxies, four galaxies have consistent classes for both nuclei and are assigned composite (3/4) and Seyfert 2 (1/4) classes, respectively. The remaining five double-nuclei galaxies have a composite nucleus plus either a starburst nucleus (4/5) or a Seyfert 2 nucleus (1/5). Because their overall class is uncertain, we exclude these five double-nuclei galaxies from our sample. We note that our results are unchanged if we randomly assign these double-nuclei galaxies the class of either nucleus.

The BGS sample covers lower IR luminosities than the 1 Jy ULIRG sample and has a larger portion of star-forming galaxies. The 2-of-3 classification scheme gives 30 (25.97%) star-forming galaxies, 32 (41.56%) starburst–AGN composites, 19 (24.67%) Seyfert 2, one (1.3%) Seyfert 1, and five (6.5%) LINERs. These classifications include 13 galaxies with double nuclei in which both nuclei have consistent classes (7/13 star forming and 6/13 composites). We do not include an additional five double-nuclei galaxies with differing classes for each nucleus. Our results are not affected if we randomly assign these double-nuclei galaxies the class of either nucleus.

There are 175 galaxies in the SW01 sample that have measured emission-line ratios with signal-to-noise ratio S/N $> 3\sigma$. The SW01 sample covers substantially IR lower luminosities than the BGS or 1 Jy ULIRG samples and contains a large fraction of star-forming galaxies. In the 2-of-3 scheme, the SW01 sample contains 78 (41.7%) star-forming galaxies, 57 (30.5%) starburst–AGN composites, 40 (21.4%) Seyfert 2, 10 (5.3%) Seyfert 1, and two (1.1%) LINERs. These statistics include 12 double-nuclei galaxies with consistent classifications for both nuclei (7/12 star-forming galaxies, 3/12 composites, and 2/12 Seyfert 2 galaxies). We do not include four double-nuclei galaxies that have different spectral types for each nucleus. Our results remain unchanged if we randomly assign these four galaxies the class of either nucleus.

Our classifications for the 1 Jy ULIRG, BGS, and SW01 samples are listed in Tables 1, 2, and 3, respectively. For comparison, in Tables 1 and 2, we also list the classifications given in Veilleux et al. (1999) using the traditional VO87 method.

### 2.3. AGN Contribution

Ke06 showed that the SDSS galaxies form a mixing sequence between pure star-forming galaxies and pure AGN. They defined an empirical linear distance ($D_{\rm SF}$) from the star-forming sequence for both the Seyfert and LINER branches on the [O III]/H$\beta$ versus [O I]/H$\alpha$ diagnostic diagram. The [O III]/H$\beta$ versus [O I]/H$\alpha$ diagram was used to derive this distance because in this diagram, the Seyfert and LINER branches are clearly separated (unlike the [O III]/H$\beta$ versus [N II]/H$\alpha$ diagram where the Seyfert and LINER branches coincide). Figure 2 shows that unlike the optically selected SDSS galaxies the majority of IR-selected galaxies do not lie along the pure star-forming galaxy sequence; most IR galaxies lie in the composite and AGN regions of the diagnostic diagrams. Because of this difference, it is more intuitive to think of the linear distance between the star-forming sequence and the AGN region on the [O III]/H$\beta$ versus [O I]/H$\alpha$ diagnostic diagram as the relative contribution of $D_{\rm AGN}$ for IR-selected galaxies.

The quantity $D_{\rm AGN}$ can be defined using other standard diagnostic diagrams with negligible difference. In Appendix A, we investigate alternative definitions of $D_{\rm AGN}$, and the relationship between $D_{\rm AGN}$ and spectral class. Because $D_{\rm AGN}$ is a relative measure, our results remain the same regardless of how $D_{\rm AGN}$ is defined. Note that because $D_{\rm AGN}$ is defined as a distance (in dex) in log line-ratio space, it does not give the fraction or a percentage of star formation or AGN emission in a galaxy. $D_{\rm AGN}$ gives a *relative* indication of the relative contribution of AGN to the EUV radiation field from galaxy to galaxy. The absolute value of $D_{\rm AGN}$ is abstract, and $D_{\rm AGN}$ should be used only in relation to other galaxies. For example, a galaxy with $D_{\rm AGN} = 0.6$ does not correspond to an AGN contribution of 60%. $D_{\rm AGN}$ is useful only for relative comparisons, for example, a galaxy with $D_{\rm AGN} = 0.6$ is likely to have a larger contribution from an AGN than a galaxy with a smaller $D_{\rm AGN}$.

In Figure 3, we show $D_{\rm AGN}$ on the [O III]/H$\beta$ versus [O I]/H$\alpha$ diagram, relative to the Ke06 classification scheme (red lines). By definition, $D_{\rm AGN} = D_{\rm SF}$ from Ke06. Pure star-forming galaxies have $D_{\rm AGN} = 0$. The mixing sequence from pure star-forming galaxies to the tip of the AGN branch begins at $D_{\rm AGN} \geqslant 0$, and lies below the maximum starburst line (red curve in Figure 3). Galaxies that are classed as composites in the [O III]/H$\beta$ versus [N II]/H$\alpha$ diagram have $D_{\rm AGN} \leqslant 0.5$ or 0.6 (green curve). Galaxies that have $D_{\rm AGN} = 1$ are likely to have line ratios that are strongly dominated by an AGN, although some contribution from star formation cannot be ruled out.

### 2.4. Merger Progress Tracers

We use two tracers of merger progress: merger morphology, and projected nuclear separation (*ns*). We adopt the morphological classification scheme outlined in Veilleux et al. (2002). Veilleux et al. (2002) relate galaxy morphology to merger stage using numerical simulations of galaxy mergers (Barnes & Hernquist 1992, 1996).

1. Wide binary: "binary systems" with projected separation $ns > 10$ kpc.
2. Close binary: "binary systems" with projected separation $ns < 10$ kpc.
3. Diffuse merger: single systems ($ns \sim 0$) with tidal features, and with $L_{K\,4\,\rm kpc}/L_K < 1/3$, where $L_{K\,4\,\rm kpc}$ means the *K*-band luminosity within 4 kpc and $L_K$ is the total luminosity.
4. Compact merger: single systems ($ns \sim 0$) with tidal features, and with $L_{K\,4\,\rm kpc}/L_K > 1/3$.

**Table 1**
Spectral Classification Result for the 1 Jy ULIRG Sample

| Name | Spectral Type | | | | | $D_{AGN}$ | Morphology | $\log(L_{IR}/L_{\odot})$ |
|---|---|---|---|---|---|---|---|---|
| *IRAS* FSC | [N II] | [S II] | [O I] | Adopt | VO87 | | Class | |
| (1) | (2) | (3) | (4) | (5) | (6) | (7) | (8) | (9) |
| 00091−0738 | cp | H | H | cp | H: | 0.1 (0.2) | b | 12.19 |
| 00188−0856 | S2 | H | S2 | S2: | L | 0.7(0.8) | e | 12.33 |
| 00397−1312 | cp | H | H | cp | H | 0.4 (0.3) | e | 12.90 |
| 00456−2904 | cp | H | H | cp | H | 0.2 (0.3) | a | 12.12 |
| 00482−2721 | cp | H: | L | cp: | L: | 0.8 (0.5) | b | 12.00 |
| 01004−2237 | cp | S2 | S2 | S2: | H: | 0.7 (0.4) | e | 12.24 |
| 01166−0844 | H:: | H | ... | H: | H: | 0 (0.2) | b | 12.03 |
| 01199−2307 | H: | H: | S2: | H: | H: | 0.6 (1) | a | 12.26 |
| 01298−0744 | cp | H | L | cp: | H: | 0.6 (0.3) | d | 12.27 |
| 01355−1814 | cp | H | H | cp | H | 0.3 (0.3) | b | 12.39 |
| 01569−2939 | cp | H | S2 | cp: | H: | 0.6 (0.4) | c | 12.15 |
| 01572+0009(MRK1014) | ... | ... | ... | S1 | S1 | 1 (1) | d | 12.53 |
| 02411+0353:main | cp | H | H | cp | H | 0.3 (0.3) | b | 12.19 |
| 02411+0353:E | H | H | H | H | H | 0 (0.4) | b | ... |
| 02411+0353:W | H | H | H | H | H | 0 (0.2) | b | ... |
| 03209−0806 | cp | H | H: | cp | H: | 0.4 (0.4) | d | 12.191 |
| 03250+1606 | cp | H | S2 | cp: | L | 0.6 (0.5) | d | 12.06 |
| Z03521+0028 | S2:: | S2: | S2: | S2 | L | 0.6 (0.6) | b | 12.45 |
| 04074−2801 | L: | L | L | L | L | 0.9 (0.6) | c | 12.14 |
| 04103−2838 | S2 | H | S2 | S2: | L: | 0.7 (0.6) | d | 12.15 |
| 05020−2941 | cp:: | H: | S2: | cp: | L: | 0.4 (0.3) | c | 12.28 |
| 05024−1941 | S2:: | S2: | S2: | S2 | S2 | 0.9 (1) | c | 12.43 |
| 05156−3024 | S2 | S2 | S2: | S2 | S2 | 1 (1) | d | 12.20 |
| 05189−2524 | S2 | S2 | S2 | S2 | S2 | 1 (1) | d | 12.07 |
| 07599+6508 | ... | ... | ... | S1 | S1 | 1 (1) | d | 12.46 |
| 08201+2801 | cp | H | H | cp | H | 0.3 (0.3) | c | 12.23 |
| 08559+1053 | S2 | S2 | S2 | S2 | S2 | 0.8 (0.8) | d | 12.16 |
| 08572+3915:NW | cp | S2 | S2 | S2: | L: | 0.6 (0.4) | b | 12.11 |
| 08572+3915:SE | S2 | S2 | H | S2: | L: | 0.5(0.7) | b | ... |
| 09039+0503 | cp | H | L | cp: | L | 0.5 (0.5) | c | 12.07 |
| 09116+0334 | S2:: | H | S2 | S2: | L: | 0.6 (0.6) | a | 12.11 |
| 09463+8141 | S2:: | L: | S2: | S2: | L | 0.7 (0.5) | c | 12.29 |
| 09539+0857 | S2 | S2 | L | S2: | L | 0.8 (0.6) | e | 12.03 |
| 10091+4704 | cp | L | L | L: | L: | 0.5 (0.5) | c | 12.67 |
| 10190+1322 | H | H | H | H | H | 0 (0.2) | b | 12.00 |
| 10378+1108 | S2 | H: | S2 | S2: | L | 0.6 (0.6) | d | 12.26 |
| 10485−1447 | S2:: | H: | S2: | S2: | L: | 0.8 (0.5) | a | 12.17 |
| 10494+4424 | cp | H | L | cp: | L | 0.6 (0.4) | d | 12.13 |
| 10594+3818 | cp: | H: | H: | cp | H | 0.3 (0.3) | b | 12.24 |
| 11028+3130 | cp | H | L | cp: | L | 0.5 (0.6) | c | 12.32 |
| 11095−0238 | cp | H | L | cp: | L | 0.6 (0.4) | d | 12.20 |
| 11119+3257 | ... | ... | ... | S1 | S1 | 1 (1) | d | 12.58 |
| 11130−2659 | cp:: | H: | L: | cp: | L | 0.7 (0.5) | c | 12.05 |
| 11180+1623 | cp: | H: | L: | cp: | L: | 0.5 (0.4) | a | 12.24 |
| 11223−1244 | S2 | S2 | S2 | S2 | S2 | 1 (1) | a | 12.59 |
| 11387+4116 | S2 | H | H | H: | H: | 0.4 (0.5) | e | 12.18 |
| 11506+1331 | cp | H | L | cp: | H: | 0.6(0.3) | d | 12.28 |
| 11582+3020 | cp | H | L | cp: | L | 0.6 (0.5) | e | 12.56 |
| Z11598−0112 | ... | ... | ... | S1 | S1 | 1 (1) | d | 12.43 |
| 12032+1707 | S2 | H | S2 | S2: | L | 0.7 (0.6) | d | 12.57 |
| 12072−0444 | S2 | S2 | S2 | S2 | S2 | 0.9 (0.8) | d | 12.35 |
| 12112+0305 | S2 | S2 | S2 | S2 | L | 0.7 (0.5) | b | 12.28 |
| 12127−1412 | S2:: | H: | H: | H: | L: | 0.4 (0.6) | a | 12.10 |
| 12265+0219(3C273) | | ... | ... | S1 | S1 | 1 (1) | d | 12.73 |
| 12359−0725:N | cp | H | L | cp: | L | 0.7 (0.5) | a | 12.11 |
| 12359−0725:S | H | H | H | H | H | 0 (0.2) | a | ... |
| 12447+3721 | cp: | H: | H: | cp | H | 0.5 (0.3) | c | 12.06 |
| 12540+5708(MRK0231) | ... | ... | ... | S1 | S1 | 1 (1) | d | 12.50 |
| 13106−0922 | cp | H | L | cp: | L: | 0.7 (0.4) | c | 12.32 |
| 13218+0552 | ... | ... | ... | S1 | S1 | 1(1) | e | 12.63 |
| 13305−1739 | S2: | S2: | S2: | S2 | S2 | 1 (0.9) | e | 12.21 |
| 13335−2612 | cp | H | S | cp: | L: | 0.5 (0.4) | b | 12.06 |
| 13342+3932 | ... | ... | ... | S1 | S1 | 1 (1) | d | 12.37 |
| 13428+5608(MRK0273) | S2 | S2 | S2 | S2 | S2 | 0.8 (0.8) | d | 12.10 |

**Table 1**
(Continued)

| Name | Spectral Type | | | | | $D_{AGN}$ | Morphology | $\log(L_{IR}/L_{\odot})$ |
|---|---|---|---|---|---|---|---|---|
| *IRAS* FSC | [N II] | [S II] | [O I] | Adopt | VO87 | | Class | |
| (1) | (2) | (3) | (4) | (5) | (6) | (7) | (8) | (9) |
| 13443+0802:NE | cp | H: | H | cp | H | 0.2 (0.3) | tpl | 12.15 |
| 13443+0802:SW | S2 | S2: | S2 | S2 | S2 | 1 (1) | tpl | ... |
| 13451+1232 | S2 | S2 | S2 | S2 | S2 | 1(0.9) | b | 12.28 |
| 13454−2956 | S2 | S2 | S2 | S2 | S2 | 0.8 (0.8) | a | 12.21 |
| 13469+5833 | cp: | H: | H: | cp | H | 0.1 (0.3) | b | 12.15 |
| 13509+0442 | cp | H: | H | cp | H | 0.4 (0.2) | d | 12.27 |
| 13539+2920 | cp | H | H | cp | H: | 0.5 (0.3) | b | 12.00 |
| 14053−1958 | L:: | L: | L: | L | S2 | 1 (0.8) | b | 12.12 |
| 14060+2919 | cp | H | H | cp | H | 0.2 (0.3) | c | 12.03 |
| 14070+0525 | S2 | S2 | S2 | S2 | S2 | 0.8 (0.7) | e | 12.76 |
| 14121−0126 | S2 | H | S2 | S2: | L | 0.7 (0.7) | b | 12.23 |
| 14202+2615 | cp | H | H | cp | H | 0.2 (0.3) | a | 12.39 |
| 14252−1550 | cp:: | H | H | cp | L: | 0.5 (0.4) | b | 12.15 |
| 14348−1447:SW | cp | S2 | L | cp:: | L | 0.7 (0.5) | b | 12.28 |
| 14348−1447:NE | cp | H | L | cp: | L | 0.6 (0.5) | b | ... |
| 14394+5332 | S2 | S2 | L | S2: | S2 | 0.9 (0.7) | tpl | 12.04 |
| 15001+1433 | S2 | S2 | S2 | S2 | S2 | 0.7 (0.6) | tpl | 12.38 |
| 15043+5754 | H | H | H | H | H | 0 (0.2) | b | 12.05 |
| 15130−1958 | S2 | S2 | S2 | S2 | S2 | 1 (1) | d | 12.09 |
| 15206+3342 | cp | H | H | cp | H | 0.6 (0.3) | d | 12.18 |
| 15225+2350 | cp | H | S2 | cp: | H: | 0.6 (0.5) | a | 12.10 |
| 15327+2340(Arp220) | L | L | L | L | L | 0.7 (0.9) | b | 12.17 |
| 15462−0450 | ... | ... | ... | S1 | S1 | 1(1) | d | 12.16 |
| 16090−0139 | cp | H | H | cp | L: | 0.5 (0.5) | c | 12.49 |
| 16156+0146 | S2 | S2: | S2 | S2 | S2 | 1 (1) | b | 12.04 |
| 16300+1558 | cp | H | L | cp: | L | 0.6 (0.4) | e | 12.63 |
| 16333+4630 | cp | H | S2 | cp: | L | 0.5 (0.4) | a | 12.35 |
| 16468+5200:W | cp | H | H | cp | L: | 0.2 (0.4) | b | 12.02 |
| 16468+5200:E | cp | L | H | cp: | L | 0.4 (0.4) | b | ... |
| 16474+3430 | cp | H | H | cp | H: | 0.4 (0.3) | b | 12.11 |
| 16487+5447 | cp | H | S2 | cp: | L: | 0.5 (0.5) | b | 12.12 |
| 17028+5817:W | cp | H | H | cp | L: | 0.6 (0.4) | a | 12.10 |
| 17028+5817:E | H | H | H | H | H | 0 (0.1) | a | ... |
| 17044+6720 | S2 | S2 | S2 | S2 | L | 0.7 (0.6) | d | 12.13 |
| 17068+4027 | cp | H | H | cp | H | 0.5(0.3) | tpl | 12.30 |
| 17179+5444 | S2 | S2 | S2 | S2 | S2 | 1 (1) | d | 12.20 |
| 20414−1651 | cp | H | L | cp: | H: | 0.5 (0.3) | d | 12.14 |
| 21208−0519:N | cp | H: | H | cp | H | 0.2 (0.3) | a | 12.01 |
| 21208−0519:S | cp | H: | H | cp | H: | 0.4 (0.4) | a | ... |
| 21219−1757 | ... | ... | ... | S1 | S1 | 1 (1) | e | 12.06 |
| 21329−2346 | cp | H | L | cp: | L | 0.5 (0.4) | d | 12.09 |
| 21477+0502 | cp | H: | L | cp: | L: | 0.6 (0.4) | tpl | 12.24 |
| 22088−1831 | H | H: | H: | H | H: | 0 (0.2) | b | 12.31 |
| 22206−2715 | cp | H | L | cp: | H: | 0.5 (0.3) | b | 12.19 |
| 22491−1808 | H | H | H | H | H | 0 (0.2) | b | 12.09 |
| 22541+0833:NW | cp | L: | H | cp: | L: | 0.4 (0.5) | a | 12.23 |
| 22541+0833:SE | ... | ... | ... | ... | S2: | ... (...) | a | ... |
| 23060+0505 | S2 | S2 | S2: | S2 | S2 | 0.9 (0.8) | d | 12.44 |
| 23129+2548 | cp:: | H | L: | cp: | L: | 0.5 (0.4) | c | 12.38 |
| 23233+2817 | S2 | S2 | S2 | S2 | S2 | 1 (1) | iso | 12.00 |
| 23234+0946 | cp | H | L: | cp: | L | 0.6 (0.5) | b | 12.05 |
| 23327+2913 | S2 | H | S2: | S2: | L: | 0.6 (0.6) | a | 12.06 |
| 23389+0300 | S2: | S2: | L: | S2: | S2 | 1 (1) | b | 12.09 |
| 23498+2423 | S2 | S2 | S2: | S2 | S2 | 0.9 (1) | a | 12.40 |

**Notes.** Column 1: galaxy name. Columns 2–4: optical spectral types derived in this work from the [N II] λ6583, [S II] λλ6716, 6731, and [O I] λ6300 diagrams, respectively. The typical uncertainty on the emission-line ratios is ∼10%; colons in Columns 3 and 4 indicate larger uncertainty of the line ratios of ∼25% for [S II]/H$\alpha$ and [O I]/H$\alpha$, respectively; double colons in Column 2 indicate larger uncertainty of the line ratios of ∼25% for [O III]/H$\beta$. Column 5 is the adopted spectral type using the 2-of-3 scheme; single colons indicate the object does not have the same spectral type in all three diagrams, i.e., the ambiguous class. Double colon means the classification does not agree on any of the diagrams, the classification in those rare cases is highly uncertain. For comparison, Column 6 lists the VO87 classification results (Veilleux et al. 1999). Symbols: H = star-forming galaxies, L = LINERs, S2 = Seyfert 2 galaxies, S1 = Seyfert 1 galaxies, cp = starburst–AGN composite galaxies. Column 7: $D_{AGN}$ defined on the [O I]/H$\alpha$ diagram, for comparison, in the bracket we also list the $D_{AGN}$ derived from the [N II]/H$\alpha$ diagram (see Appendix A). Column 8: morphology class as adopted from Veilleux et al. (2002). a: wide binary; b: close binary; c: diffuse merger; d: compact merger; e: old merger; tpl: triple mergers; iso: isolated. Column 9: $\log(L_{IR}/L_{\odot})$, data from Veilleux et al. (1999).

**Table 2**
Spectral Classification Result and Morphology for the *IRAS* BGS Sample

| Name | Spectral Type | | | | | $D_{AGN}$ | *ns* | Reference | Morphology | $\log(L_{IR}/L_{\odot})$ |
|---|---|---|---|---|---|---|---|---|---|---|
| | [N II] | [S II] | [O I] | Adopt | "VO87" | | (kpc) | | Class | |
| (1) | (2) | (3) | (4) | (5) | (6) | (7) | (8) | (9) | (10) | (11) |
| NGC 23 | cp | H | H | cp | H | 0.2(0.3) | −2 | 2MASS, DSS | iso | 11.05 |
| NGC 34 | S2 | S2 | S2 | S2 | S2 | 0.7(0.8) | −1 | 2MASS, DSS | cde | 11.41 |
| MCG-02-01-051:S | H:: | H | H | H | H | 0(0.2) | 27.7 | 2MASS | a | 11.32 |
| MCG-02-01-051:N | H | H | H | H | H | 0(0.1) | 27.7 | 2MASS | a | ... |
| NGC 232 | cp | H | H | cp | H: | 0.4(0.5) | 8.8 | 2MASS | b | 11.30 |
| UGC 556 | cp | H | L | cp: | L | 0.5(0.3) | −2 | 2MASS, DSS | iso | 10.82 |
| IC1623:N | H | H | H | H | H | 0(0.2) | 5.3 | 2MASS | b | 11.54 |
| IC1623:SE | H | H | H | H | H | 0(0.2) | 5.3 | 2MASS | b | ... |
| MCG-03-04-014 | cp | H | H | cp | H | 0.1(0.2) | −2 | 2MASS, DSS | iso | 11.58 |
| MCG+02-04-025 | H | H | H | H | H | 0(0.2) | −1 | 2MASS, DSS | cde | 11.63 |
| UGC903 | cp | H | H | cp | H: | 0.2(0.3) | −2 | 2MASS, DSS | iso | 10.37 |
| NGC 520 | ... | ... | ... | ... | ... | ... | ... | ... | ... | 10.88 |
| IR01364-1042 | L:: | L: | L: | L | L | 0.8(0.6) | −1 | 2MASS, DSS | cde | 11.76 |
| NGC 660 | S2 | S2 | S2 | S2 | L | 0.6(0.7) | −2 | 2MASS, DSS | iso | 10.47 |
| IIIzw 35:S | S2:: | H | S2 | S2: | L | 0.7(0.6) | ... | 2MASS, DSS | ... | 11.54 |
| IIIzs 35:N | H | H | H | H | H | 0(0.1) | ... | 2MASS, DSS | ... | ... |
| NGC 695 | H | H | H | H | H | 0(0.2) | −2 | 2MASS, DSS | iso | 11.64 |
| NGC 873 | H | H | H | H | H | 0(0.2) | −2 | 2MASS, DSS | iso | 10.60 |
| NGC 1050 | cp | H | H | cp | H | 0.1(0.3) | −2 | 2MASS, DSS | iso | 10.72 |
| NGC 1056 | H | H | H | H | H | 0(0.2) | −2 | 2MASS, DSS | iso | 9.92 |
| NGC 1068 | S2: | S2: | S2: | S2 | S2 | 1(1) | −2 | 2MASS, DSS | iso | 11.27 |
| NGC 1083 | H | H | H | H | H | 0(0.2) | −2 | 2MASS, DSS | iso | 10.76 |
| UGC2238 | cp:: | H: | S2 | cp: | L: | 0.6(0.5) | ... | 2MASS, DSS | ... | 11.24 |
| IR02438+2122 | S2:: | H: | S2 | S2: | L | 0.8(0.8) | ... | 2MASS, DSS | ... | 11.08 |
| UGC2369 | cp | H | H | cp | H | 0.2(0.3) | 11.5 | 2MASS | a | 11.58 |
| NGC 1143/4 | S2 | S2 | S2 | S2 | S2 | 1(1) | 13.3 | 2MASS | a | 11.39 |
| UGC2403 | cp | H | H | cp | H | 0.2(0.3) | −2 | 2MASS, DSS | iso | 10.86 |
| NGC 1204 | cp | H | H | cp | L: | 0.3(0.4) | −2 | 2MASS, DSS | iso | 10.81 |
| NGC 1266 | L:: | L | L | L | L | 0.8(1) | −2 | 2MASS, DSS | iso | 10.34 |
| NGC 1377 | ... | ... | ... | ... | ... | ... | ... | ... | ... | 10.04 |
| IR03359+1523 | H | H | H | H | H | 0(0.2) | 6.9 | 2MASS | b | 11.47 |
| UGC2982 | H | H | H | H | H | 0(0.1) | −2 | 2MASS, DSS | iso | 11.15 |
| ESO550-IG025:S | cp | H | H | cp | L: | 0.3(0.4) | 4.5 | 2MASS | b | 11.44 |
| ESO550-IG025:N | cp | H | L | cp: | L | 0.4(0.4) | 4.5 | 2MASS | b | ... |
| NGC 1614 | cp | H | H | cp | H: | 0.2(0.4) | −1 | 2MASS, DSS | cde | 11.58 |
| ESO484-G036 | ... | ... | ... | ... | ... | ... | ... | ... | ... | 10.80 |
| ESO485-G003 | H | H | H | H | H | 0(0.1) | −2 | 2MASS, DSS | iso | 10.82 |
| IC398 | ... | ... | ... | ... | ... | ... | ... | ... | ... | 10.82 |
| NGC 1797 | H | H | H | H | H | 0(0.2) | −2 | 2MASS, DSS | iso | 10.97 |
| IR05187-1017 | L:: | L | L | L | L | 0.6(0.7) | −2 | 2MASS, DSS | iso | 11.23 |
| ∗IR05189-2524 | S2:: | S2 | S2 | S2 | S2 | 1(1) | −2 | 2MASS, DSS | iso | 12.09 |
| NGC 2388 | H | H | H | H | H | 0(0.2) | 59.5 | DSS | a | 11.18 |
| IR08339+6517 | H | H | H | H | H | 0(0.2) | −2 | 2MASS, DSS | iso | 11.08 |
| NGC 2623 | ... | ... | ... | ... | ... | ... | ... | ... | ... | 11.55 |
| ∗IR08572+3915 | cp | L | S2 | cp:: | L: | 0.5(0.4) | 59.1 | 2MASS | a | 12.11 |
| NGC 2785 | cp | H | H | cp | H | 0.3(0.3) | 86.5 | DSS | a | 10.70 |
| UGC4881:SW | cp | H | H | cp | H: | 0.3(0.3) | 8.3 | 2MASS | b | 11.70 |
| UGC4881:NE | cp:: | H | H | cp | H: | 0.2(0.3) | 8.3 | 2MASS | b | ... |
| UGC5101 | S2 | H | S2 | S2: | L | 0.6(0.8) | −1 | 2MASS, DSS | cde | 12.00 |
| MCG+08-18-012 | cp | H | H | cp | H: | 0.3(0.3) | 30.4 | 2MASS | a | 11.31 |
| NGC 3110 | H | H | H: | H | H | 0(0.1) | 100: | 2MASS, DSS | a iso | 11.22 |
| IR10565+2448:W | cp | H | H | cp | H | 0.2(0.2) | 20.1 | 2MASS, DSS | a | 12.00 |
| IR10565+2448:NE | ... | ... | ... | ... | ... | ... | ... | ... | ... | ... |
| NGC 3508:W | H | H | H | H | H | 0(0.1) | ... | 2MASS, DSS | ... | 10.79 |
| NGC 3508:E | H | H | H: | H | H | 0(0) | ... | 2MASS, DSS | ... | ... |
| NGC 3597 | H | H | H: | H | H | 0(0.2) | −1 | 2MASS, DSS | cde | 10.91 |
| MCG+00-29-023 | cp | H | H | cp | H: | 0.4(0.5) | −2 | 2MASS, DSS | iso | 11.23 |
| UGC6436:NW | H | H | H | H | H | 0(0.2) | 44.4 | 2MASS, DSS | a | 11.52 |
| UGC6436:SE | ... | ... | ... | ... | ... | ... | ... | ... | ... | ... |
| IR12224-0624 | S2:: | H | ... | S2:: | L: | 1(0.6) | −1 | 2MASS, DSS | cde | 11.18 |
| NGC 4666 | S2 | S2 | H: | S2: | L | 0.4(0.7) | −2 | 2MASS, DSS | iso | 11.08 |
| IC3908 | H | H | H: | H | H | 0(0.1) | −2 | 2MASS, DSS | iso | 9.45 |
| ∗UGC8058 | | | | S1 | S1 | 1(1) | −2 | 2MASS, DSS | iso | 12.53 |
| NGC 4922 | S2 | S2 | S2 | S2 | L | 0.6(0.6) | 9.4 | 2MASS | b | 11.25 |

**Table 2**
(Continued)

| Name | Spectral Type | | | | | $D_{AGN}$ | *ns* | Reference | Morphology | $\log(L_{IR}/L_{\odot})$ |
|---|---|---|---|---|---|---|---|---|---|---|
| | [N II] | [S II] | [O I] | Adopt | "VO87" | | (kpc) | | Class | |
| (1) | (2) | (3) | (4) | (5) | (6) | (7) | (8) | (9) | (10) | (11) |
| MCG-02-33-098:W | H | H | H | H | H: | 0(0.1) | 3.3 | 2MASS | b | 11.05 |
| MCG-02-33-098:E | H | H | H: | H | H | 0(0) | 3.3 | 2MASS | b | ... |
| IC860 | ... | ... | ... | ... | ... | ... | ... | ... | ... | 11.12 |
| UGC8335:NW | cp | H | H | cp | H: | 0.4(0.4) | 19 | 2MASS | a | 11.76 |
| UGC8335:SE | cp | H | H | cp | H | 0.3(0.3) | 19 | 2MASS | a | ... |
| UGC8387 | cp | H | L | cp: | L | 0.5(0.4) | 26.5 | 2MASS | a | 11.58 |
| NGC 5104 | cp:: | H | L | cp: | L | 0.5(0.5) | 26.5 | 2MASS | a | 11.11 |
| NGC 5218 | cp | H | L | cp | L | 0.4(0.5) | 46.1 | 2MASS | a | 10.69 |
| NGC 5256:SW | cp | H | L | cp | L | 0.6(0.5) | ... | 2MASS, DSS | ... | 11.48 |
| NGC 5256:NE | S2 | S2 | S2 | S2 | S2 | 0.7(0.7) | ... | 2MASS, DSS | ... | ... |
| NGC 5257/8:W | H | H | H | H | H | 0(0.2) | 100: | 2MASS, DSS | a(iso?) | 11.51 |
| NGC 5257/8:E | ... | ... | ... | ... | ... | ... | ... | ... | ... | ... |
| *UGC8696 | S2 | S2 | S2 | S2 | L | 0.7(0.7) | −1 | 2MASS, DSS | cde | 12.14 |
| NGC 5430 | H | H | H | H | H | 0(0.2) | −2 | 2MASS, DSS | iso | 10.88 |
| Zw247.020 | cp | H | H | cp | H: | 0.1(0.4) | −2 | 2MASS, DSS | iso | 11.32 |
| NGC 5653:W | H | H | H | H | H | 0(0.1) | ... | 2MASS, DSS | ... | 11.01 |
| NGC 5653:E | H:: | H | H: | H | H | 0(0) | ... | 2MASS, DSS | ... | ... |
| NGC 5676 | H | H | ... | H: | H | 0(0.2) | −2 | 2MASS, DSS | iso | 10.77 |
| *IR14348-1447:SW | cp | H | S2 | cp: | L: | 0.6(0.4) | −1 | 2MASS, DSS | cde | 12.26 |
| *IR14348-1447:NE | cp | H | L | cp: | L: | 0.6(0.4) | −1 | 2MASS, DSS | cde | ... |
| NGC 5734 | ... | ... | ... | ... | ... | ... | ... | ... | ... | 11.01 |
| UGC9618 | cp | H | L | cp: | L: | 0.5(0.5) | 25.1 | 2MASS | a | 11.65 |
| Zw049.057 | H:: | H | H: | H | H | 0(0) | −2(cl) | 2MASS, DSS | iso | 11.15 |
| I Zw107:S | cp | H | S2 | cp: | L | 0.5(0.5) | 5.4 | 2MASS | b | 11.85 |
| I Zw107:N | cp | H | H | cp | H | 0.3(0.4) | 5.4 | 2MASS | b | ... |
| IR15250+3609 | cp | H | S2 | cp: | L: | 0.4(0.4) | −1 | 2MASS, DSS | cde | 11.97 |
| NGC 5936 | cp | H | H | cp | H | 0.1(0.3) | −2 | 2MASS, DSS | iso | 11.02 |
| NGC 5953 | S2 | H | S2 | S2: | L | 0.5(0.6) | 5.5 | 2MASS | b | 10.62 |
| *UGC9913:S | ... | ... | ... | ... | ... | ... | ... | ... | ... | 12.18 |
| *UGC9913:N | S2:: | S2 | S2 | S2 | S2 | 1(1) | ... | | cde | ... |
| IR15335-0513 | S2:: | H | S2 | S2: | L | 0.6(0.6) | −2 | 2MASS, DSS | iso | 11.25 |
| NGC 6090:SW | H | H | H | H | H | 0(0.2) | 3.6 | 2MASS | b | 11.49 |
| NGC 6090:NE | H | H | H | H | H | 0(0.1) | 3.6 | 2MASS | b | ... |
| IR16164-0746 | S2 | H | S2 | S2: | L | 0.7(0.6) | −1 | 2MASS, DSS | cde | 11.43 |
| MCG+01-42-088 | H | H | H | H | H | 0(0.2) | ... | ... | ... | 11.34 |
| NGC 6181 | H:: | H | ... | H: | H | ... (0.1) | −2(cl) | 2MASS, DSS | iso | 10.69 |
| NGC 6240 | L | L | L | L | L | 0.8(0.7) | 0.74 | tec00 | b | 11.83 |
| NGC 6285/6:NW | cp | H | H | cp | H: | 0.3(0.2) | 31.3 | 2MASS | a | 11.33 |
| NGC 6285/6:SE | cp | H | L | cp: | L | 0.5(0.5) | 31.3 | 2MASS | a | ... |
| IR17132+5313:W | ... | ... | ... | ... | ... | ... | ... | ... | ... | 11.88 |
| IR17132+5313:E | H | H | H | H | H | 0(0.2) | 6 | 2MASS | b | ... |
| IR17138-1017 | ... | ... | ... | ... | ... | ... | ... | ... | ... | 11.39 |
| *IR17208-0014 | H | H | H | H | H | 0(0.2) | −1 | 2MASS, DSS | cde | 12.40 |
| NGC 6621[a] | H | H | H | H | H | 0(0.3) | 15.7 | 2MASS | a | 11.26 |
| IR18293-3413 | H | H | H | H | H | 0(0.2) | 100: | 2MASS, DSS | iso | 11.26 |
| NGC 6670:W | H | H | H | H | H | 0(0) | m | 2MASS, DSS | m | 11.60 |
| NGC 6670:E | H:: | H | H | H | H | 0(0.2) | m | 2MASS, DSS | m | ... |
| NGC 6701 | cp | H | H | cp | H: | 0.4(0.4) | −2 | 2MASS, DSS | iso | 11.09 |
| ESO593-IG008:S | S2 | H:: | S2 | S2: | L | 0.4(1) | ... | 2MASS, DSS | ... | 11.86 |
| ESO593-IG008:N | cp | H | H | cp | H | 0.2(0.3) | ... | 2MASS, DSS | ... | ... |
| *IR19297-0406 | cp | H | H | cp | H | 0.4(0.3) | m | 2MASS, DSS | m | 12.36 |
| NGC 6926 | S2:: | S2 | L | S2: | S2 | 1(0.9) | −2 | 2MASS, DSS | iso | 11.27 |
| Zw448.020:NW | ... | ... | ... | ... | ... | ... | ... | ... | ... | 11.89 |
| Zw448.020:SE | H | H | H | H | H | 0(0.2) | 6.7 | 2MASS | b | ... |
| ESO286-IG019 | H | H | H | H | H: | 0(0.2) | −1 | 2MASS | cde | 11.98 |
| ESO343-IG013:S | cp | H | H | cp | H: | 0.2(0.3) | 3.9 | 2MASS | b | 11.05 |
| ESO343-IG013:N | cp | H | H | cp | H | 0.2(0.2) | 3.9 | 2MASS | b | ... |
| NGC 7130 | S2 | S2 | L | S2: | L | 0.9(0.7) | −2 | 2MASS, DSS | iso | 11.31 |
| IC5179 | H:: | H | H | H | H | 0(0) | −2 | 2MASS, DSS | iso | 11.12 |
| ESO602-G025 | cp | H | H | cp: | L: | 0.4(0.4) | −2 | 2MASS, DSS | iso | 11.25 |
| ESO534-G009 | L:: | L | L | L | L | 0.8(0.9) | −2 | 2MASS, DSS | iso | 10.61 |
| UGC12150 | cp | H | H | cp | H: | 0.1(0.3) | −2 | 2MASS, DSS | iso | 11.29 |
| *IR22491-1808 | H | H | H | H | H | 0(0.2) | 3.9 | 2MASS | b | 12.08 |
| NGC 7469 | | | | S1 | S1 | 1(1) | 19 | 2MASS | a | 11.60 |

**Table 2**
(Continued)

| Name | Spectral Type | | | | | $D_{AGN}$ | *ns* | Reference | Morphology | $\log(L_{IR}/L_{\odot})$ |
|---|---|---|---|---|---|---|---|---|---|---|
| | [N II] | [S II] | [O I] | Adopt | "VO87" | | (kpc) | | Class | |
| (1) | (2) | (3) | (4) | (5) | (6) | (7) | (8) | (9) | (10) | (11) |
| Zw453.062 | S2 | H | S2 | S2: | L | 0.6(0.7) | −2 | 2MASS, DSS | iso | 11.28 |
| Zw475.056 | S2 | S2 | S2 | S2 | S2 | 0.7(0.8) | −2 | 2MASS, DSS | iso | 11.53 |
| NGC 7591 | S2 | H | S2 | S2: | L | 0.5(0.6) | −2 | 2MASS, DSS | iso | 11.04 |
| NGC 7592:W | S2 | S2 | S2 | S2 | S2 | 0.7(0.7) | 23.7 | 2MASS | a | 11.33 |
| NGC 7592:E | H | H | H | H | H | 0(0.1) | 23.7 | 2MASS | a | ... |
| NGC 7674 | S2 | S2 | S2 | S2 | S2 | 1(1) | 17.4 | 2MASS | a | 11.49 |
| NGC 7679 | S2 | S2 | S2 | S2 | S2 | 0.7(0.7) | −2 | 2MASS, DSS | iso | 11.05 |
| NGC 7714 | cp | H | H | cp | H | 0.4(0.3) | 15.5 | 2MASS | a | 10.67 |
| ∗IR23365+3604 | cp | H | H | cp | L | 0.3(0.4) | −2 | 2MASS, DSS | iso | 12.14 |
| NGC 7771 | cp | H | H: | cp | H | 0.3(0.3) | 16.8 | 2MASS | a | 11.35 |
| NGC 7771:S | H | H | H | H | H | 0(0.2) | 16.8 | 2MASS | a | ... |
| MCG+03-60-036 | H | H | H | H | H | 0(0.3) | 100: | 2MASS, DSS | iso | 11.41 |

**Notes.** Column 1: galaxy name. ∗ denotes ULIRGs. Columns 2–4: optical spectral types derived in this work from the [N II] λ6583, [S II] λλ6716, 6731, and [O I] λ6300 diagrams, respectively. The typical uncertainty on the emission-line ratios is ∼10%; colons in Columns 3 and 4 indicate larger uncertainty of the line ratios of ∼25% for [S II]/H$\alpha$ and [O I]/H$\alpha$, respectively; double colons in Column 2 indicate larger uncertainty of the line ratios of ∼25% for [O III]/H$\beta$. Column 5 is the adopted spectral type using the 2-of-3 scheme; colons indicate the object does not have the same spectral type in all three diagrams, i.e., the ambiguous class. Double colon means the classification does not agree on any of the diagrams, the classification in those rare cases is highly uncertain. For comparison, Column 6 lists the VO87 classification results (Veilleux et al. 1999). Symbols: H = star-forming galaxies, L = LINERs, S2 = Seyfert 2 galaxies, S1 = Seyfert 1 galaxies, cp = starburst–AGN composite galaxies. Column 7: $D_{AGN}$ defined on the [O I]/H$\alpha$ diagram, for comparison, in the bracket we also list the $D_{AGN}$ derived from the [N II]/H$\alpha$ diagram (see Appendix A). Column 8: projected nuclear separation in kpc. −1: single nucleus with tidal features; −2: isolated systems "": lower limit; "m": multiple (more than two) interacting objects; "cl": member of clusters. Column 9: references used to obtain projected separation or tidal features. 2MASS: 2MASS images ($K_s$ band); DSS: DSS images; tec00: Tecza et al. (2000). Column 10: adopted morphology class, a: wide binary; b: close binary; cde: single merger (either diffuse merger, compact merger, or old merger); iso: isolated system; m: multiple mergers. Column 11: $\log(L_{IR}/L_{\odot})$, data from Kim et al. (1995).

[a] Line flux of this object given in Kim et al. (1995) Table 1A has a sign error.

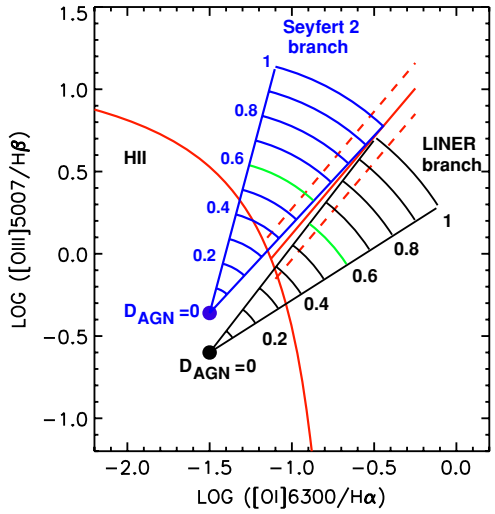


**Figure 3.** [O I]/H$\alpha$ vs. [O III]/H$\beta$ diagnostic diagram showing the Ke06 classification scheme (red lines), and the distance to the peak of the AGN branch, $D_{AGN}$. Blue and black curves give lines of constant $D_{AGN}$, respectively. The green curves indicate the maximum $D_{AGN}$ for starburst–AGN composite galaxies (defined in the [N II]/H$\alpha$ vs. [O III]/H$\beta$ diagram). Starburst galaxies and some starburst–AGN composite galaxies lie below the Ke06 maximum starburst line (red curve) in this diagram.

(A color version of this figure is available in the online journal.)

5. Old merger: single systems ($ns \sim 0$) with no unmistakable signs of tidal tails, yet have disturbed central morphologies.

We use the projected separation measured in the $K_s$ band and the length of the tidal tails measured in *R* band by Veilleux et al. (2002) for the 1 Jy sample.

For the BGS and SW01 samples, we use 2MASS $K_s$-band images and the IRAF "imcntr" task to measure the projected nuclear separations. We use *R*-band DSS images to determine the morphological classification according to the Veilleux et al. scheme. We search for companions within a 100 kpc radius. The maximum angular radius available for 2MASS images is 10 arcmin, giving galaxies at redshifts $z < 0.0087$ images less than 100 kpc wide. For these low-redshift galaxies, we use DSS images that have larger angular radii so that the 100 kpc search radius criterion is always satisfied. "Isolated systems" defined in this way are therefore confined within the 100 kpc region. It is possible that these systems are interacting with objects wider than 100 kpc. For the few galaxies without available 2MASS images, we used the data from other images in NED or from the literature. These objects are noted in Tables 1, 2, and 3.

For BGS LIRGs, we find that 42/77 are mergers, and 35/77 are isolated systems or have companions outside the 100 kpc search radius. For the remaining 37 BGS objects, the image quality is too poor for morphological classification. We do not include these 37 galaxies in the morphological study. Therefore, the morphological classification for the BGS sample is incomplete. We emphasize here that the main role of the BGS sample in this study is to supplement the 1 Jy ULIRG sample with lower luminosity objects, and to help create a larger non-ULIRGs sample in Section 3.4.

The SW01 sample is not dominated by late stage mergers (class 3, 4, 5 above) and only 33/285 can be definitively identified as mergers with $ns \sim 0$. A significant fraction (156/285) of SW01 galaxies show no obvious signs of merging or interaction. For statistical significance, we combine the

**Table 3**
Spectral Classification Result and Morphology for the SW01 Sample

| Name | Spectral Type | | | | $D_{AGN}$ | $ns$ | Reference | Morphology | $\log(L_{IR}/L_{\odot})$ |
|---|---|---|---|---|---|---|---|---|---|
| | [N II] | [S II] | [O I] | Adopt | | (kpc) | | Class | |
| (1) | (2) | (3) | (4) | (5) | (6) | (7) | (8) | (9) | (10) |
| ∗IRAS 00091−0738 | ... | ... | ... | ... | ... | −1 | 2MASS | cde | 12.16 |
| IRAS 00163−1039(Arp256) obj1 | H | H | H | H | 0(0.2) | 27.6 | 2MASS | a | 11.40 |
| IRAS 00163−1039(Arp256) obj2 | H | H | H | H | 0(0.2) | 27.6 | 2MASS | a | 11.40 |
| IRAS 00198−7926 | S2 | S2 | S2 | S2 | 0.6(0.6) | 17.5 | 2MASS | a | 11.98 |
| IRAS 00247−0203(NGC 118) | ... | ... | ... | ... | ... | −2 | 2MASS | iso | 11.35 |
| IRAS 00317−2804(NGC 150) | cp | H | H | cp | 0.4(0.4) | −2 | 2MASS | iso | 10.14 |
| IRAS 00335−2732 | cp | H | S2 | cp: | 0.5(0.4) | 6.6 | cb96 | b | 11.93 |
| IRAS 00344−3349 obj1 | H | H | H | H | 0(0.3) | 1.4 | hv94 | b | 11.18 |
| IRAS 00344−3349 obj2 | H | H | H | H | 0(0.3) | 1.4 | hv94 | b | 11.18 |
| IRAS 00366+0035(NGC 192) | cp | H | H | cp | 0.3(0.4) | 33.6 | 2MASS | a | 10.55 |
| IRAS 00450−2533(NGC 253) | cp | H | H | cp | 0.2(0.4) | 60: | DSS | a | 10.41 |
| IRAS 00510−0901(NGC 0291) | S2 | S2 | S2 | S2 | 0.9(0.9) | −2 | 2MASS | iso | 10.77 |
| IRAS 00535−5044 | H | H | H | H | 0(0) | 26.1 | 2MASS | a | 10.62 |
| IRAS 01025−6423 | cp | H | H | cp | 0.6(0.3) | −1 | 2MASS | cde | 10.75 |
| IRAS 01050−3305 | ... | ... | ... | ... | ... | 29. | 2MASS | a | 11.31 |
| IRAS 01077−1707 | ... | ... | ... | ... | ... | 41.5 | 2MASS | a | 11.56 |
| IRAS 01103−4158 | cp | H | H | cp | 0.3(0.4) | −2 | 2MASS | iso | 11.13 |
| IRAS 01159−4443 obj1 | cp | H | H | cp | 0.1(0.3) | 7.3 | 2MASS | b | 11.31 |
| IRAS 01159−4443 obj2 | cp | L | S2 | cp:: | 0.1(0.3) | 7.3 | 2MASS | b | 11.31 |
| IRAS 01165−1719 | ... | ... | ... | ... | ... | 48.5 | 2MASS | a | 10.92 |
| IRAS 01167+0418(NGC 0567) | ... | ... | ... | ... | ... | −2 | 2MASS | iso | 11.26 |
| IRAS 01171+0308(NGC 470) | H | H | H | H | 0(0.1) | −2 | 2MASS | iso | 10.39 |
| IRAS 01249−0848(MRK0995) | ... | ... | ... | ... | ... | −1 | 2MASS | cde | 11.66 |
| IRAS 01268−3551(NGC 0574) | ... | ... | ... | ... | ... | m | 2MASS | m | 10.80 |
| IRAS 01329−4141(NGC 625) | ... | ... | ... | ... | ... | −2 | 2MASS | iso | 8.48 |
| IRAS 01341−3734(NGC 633) | cp | H | H | cp | 0.2(0.3) | 21.9 | 2MASS | a | 10.94 |
| IRAS 01346+0537(NGC 632) | ... | ... | ... | ... | ... | 18.2 | DSS | a | 10.45 |
| IRAS 01348−8526 | ... | ... | ... | ... | ... | −2 | 2MASS | iso | 10.42 |
| ∗IRAS 01388−4618 | ... | ... | ... | ... | ... | −1 | 2MASS | cde | 12.03 |
| IRAS 01544−0538(NGC 762) | H | H | H | H | 0(0.2) | −2 | 2MASS | iso | 10.68 |
| IRAS 02015−2333(NGC 808) | H | H | H | H | 0(0.2) | −2 | 2MASS | iso | 10.77 |
| IRAS 02062+0744(NGC 827) | ... | ... | ... | ... | ... | −2 | 2MASS | iso | 10.52 |
| IRAS 02082−1600(NGC 814) | ... | ... | ... | ... | ... | 15.1 | DSS | a | 9.75 |
| IRAS 02092−0932(NGC 853) | ... | ... | ... | ... | ... | −2 | 2MASS | iso | 9.58 |
| IRAS 02111+0352 | ... | ... | ... | ... | ... | −2 | 2MASS | iso | 10.26 |
| IRAS 02160−0650 | cp | H | H | cp | 0.4(0.4) | 41.9 | 2MASS | a | 11.48 |
| IRAS 02242−1444 | H | H | H | H | 0(0.1) | 8.5 | vva68 | b | 10.3 |
| IRAS 02303−2954 | H | H | H | H | 0(0.1) | 100: | DSS | iso | 10.6 |
| IRAS 02304+0012 | S2 | S2 | S2 | S2 | 0.8(0.9) | −2 | 2MASS | iso | 10.88 |
| IRAS 02360−0653(NGC 1022) | H | H | H | H | 0(0.2) | 100: | 2MASS | iso | 10.38 |
| IRAS 02401−0013(NGC 1068) | S2 | S2 | S2 | S2 | 1(1) | −2 | 2MASS | iso | 11.38 |
| IRAS 02493−1651 | ... | ... | ... | ... | ... | 10.5 | 2MASS | a | 10.3 |
| IRAS 02521−1013(NGC 1140) | H | H | H | H | 0(0.1) | −2 | 2MASS | iso | 9.58 |
| IRAS 02530+0211 | cp | H | H | cp | 0.3(0.4) | −2 | 2MASS | iso | 10.99 |
| IRAS 02557−1033 | ... | ... | ... | ... | ... | 26.2 | 2MASS | a | 10.51 |
| IRAS 02572+0234 | ... | ... | ... | ... | ... | 9.2 | 2MASS | b | 10.23 |
| IRAS 03022−1232(NGC 1204) | ... | ... | ... | ... | ... | −2 | 2MASS | iso | 10.85 |
| IRAS 03064−0308(NGC 1222) | H | H | H | H | 0(0.2) | −2 | 2MASS | iso | 10.68 |
| IRAS 03144+0104 | ... | ... | ... | ... | ... | 6.6 | 2MASS | b | 10.85 |
| IRAS 03229−0618 | | | | S1 | 1(1) | 52.8 | DSS | a | 11.17 |
| IRAS 03344−2103(NGC 1377) | ... | ... | ... | ... | ... | −2 | 2MASS | iso | 9.88 |
| IRAS 03348−3609(NGC 1386) | H | H | H | H | 0(0.1) | 100: | DSS | iso | 9.35 |
| IRAS 03348−0508 | S2 | S2 | S2 | S2 | 1(1) | −2 | 2MASS | iso | 10.64 |
| IRAS 03372−1841(NGC 1042) | cp | H | H | cp | 0.2(0.4) | −2 | 2MASS | iso | 10.39 |
| IRAS 03443−1642 | ... | ... | ... | ... | ... | −2 | 2MASS | iso | 9.55 |
| IRAS 03467−2216 | cp | H | H | cp | 0.3(0.2) | −2 | 2MASS | iso | 10.55 |
| IRAS 03524−2038(NGC 1482) | ... | ... | ... | ... | ... | 100: | 2MASS | iso | 10.61 |
| IRAS 03536−1351 | ... | ... | ... | ... | ... | −1 | 2MASS | cde | 11.05 |
| ∗IRAS 03575−6132 | S2 | S2 | S2 | S2 | 0.9(1) | −1 | 2MASS | cde | 12.21 |
| IRAS 03594−6746(NGC 1511) | H | H | H | H | 0(0.1) | 100:m | 2MASS | iso | 10.19 |
| IRAS 04001−1811 | S2 | S2 | S2 | S2 | 0.6(0.6) | −2 | 2MASS | iso | 11.01 |
| IRAS 04118−3207 | S2 | H | H | H: | 0.4(0.5) | −2 | 2MASS | iso | 10.95 |
| IRAS 04131−2836(NGC 1540) obj1 | H | H | H | H | 0(0.1) | 8.7 | 2MASS | b | 10.68 |

**Table 3**
(Continued)

| Name | Spectral Type | | | | $D_{AGN}$ | *ns* | Reference | Morphology | $\log(L_{IR}/L_{\odot})$ |
|---|---|---|---|---|---|---|---|---|---|
| | [N II] | [S II] | [O I] | Adopt | | (kpc) | | Class | |
| (1) | (2) | (3) | (4) | (5) | (6) | (7) | (8) | (9) | (10) |
| IRAS 04131−2836(NGC 1540) obj2 | H | H | H | H | 0(0.1) | 8.7 | 2MASS | b | 10.68 |
| IRAS 04133+0803 | ... | ... | ... | ... | ... | −2 | 2MASS | iso | 11.49 |
| IRAS 04257−4913 | cp | H | H | cp | 0.1(0.2) | 46. | 2MASS | b | 11.75 |
| IRAS 04259−0440 | S2 | H | S2 | S2: | 0.7(0.6) | −2 | 2MASS | iso | 10.69 |
| IRAS 04273−3735 | cp | H | H | cp | 0.2(0.3) | −2 | 2MASS | iso | 10.98 |
| IRAS 04315−0840(NGC 1614) | cp | H | H | cp | 0.3(0.4) | 0.3 | 2MASS | b | 11.57 |
| IRAS 04332+0209 | ... | ... | ... | ... | ... | −2 | 2MASS | iso | 10.46 |
| IRAS 04339−1028 | | | | S1 | 1(1) | 36 | 2MASS | a | 11.32 |
| IRAS 04385−0828 | ... | ... | ... | ... | ... | −2 | 2MASS | iso | 10.67 |
| IRAS 04449−5920(NGC 1672) | ... | ... | ... | ... | ... | −2 | 2MASS | iso | 10.39 |
| IRAS 04501−3304 | cp | H | H | cp | 0.3(0.3) | −2 | 2MASS | iso | 11.07 |
| IRAS 04502+0258 | ... | ... | ... | ... | ... | 13.8 | 2MASS | a | 10.48 |
| IRAS 04520+0311(NGC 1691) | cp | H | H | cp | 0.1(0.3) | −2 | 2MASS | iso | 10.88 |
| IRAS 04591−0419 | ... | ... | ... | ... | ... | −2 | 2MASS | iso | 10.5 |
| IRAS 05053−0805(NGC 1797) | H | H | H | H | 0(0.2) | −2 | 2MASS | iso | 10.94 |
| IRAS 05059−3734(NGC 1808) | H | H | H | H | 0(0.2) | −2 | 2MASS | iso | 10.47 |
| IRAS 05066+0844 | ... | ... | ... | ... | ... | −1 | 2MASS | cde | 11.33 |
| IRAS 05095−1511 | ... | ... | ... | ... | ... | 2.6 | vva68 | b | 10.24 |
| IRAS 05100+0614 | ... | ... | ... | ... | ... | 72. | 2MASS | a | 11.40 |
| IRAS 05144−1224 | ... | ... | ... | ... | ... | −2 | 2MASS | iso | 9.65 |
| IRAS 05170+0535 | ... | ... | ... | ... | ... | −2 | 2MASS | iso | 11.78 |
| ∗IRAS 05189−2524 | ... | ... | ... | ... | ... | −1 | 2MASS | cde | 12.07 |
| IRAS 05238−4602 | S2 | S2 | S2 | S2 | 0.8(0.9) | −1 | 2MASS | cde | 11.46 |
| IRAS 05246+0103 | ... | ... | ... | ... | ... | 9. | 2MASS | b | 12.07 |
| IRAS 05409−2405 obj1 | H | H | H | H | 0(0.1) | 15. | 2MASS | a | 11.00 |
| IRAS 05409−2405 obj2 | ... | ... | ... | ... | ... | ... | 2MASS | a | 11.00 |
| IRAS 05471−4746 | S2 | S2 | S2 | S2 | 0.6(0.6) | −1 | 2MASS | cde | 11.60 |
| IRAS 05486−2259 | cp | H | H | cp | 0.3(0.4) | 1.6 | 2MASS | b | 11.05 |
| IRAS 05497−0728(NGC 2110) | L | L | L | L | 1(0.9) | −2 | 2MASS | iso | 10.08 |
| IRAS 05535−1902 | ... | ... | ... | ... | ... | −2 | 2MASS | iso | 10.12 |
| IRAS 05562−6933(NGC 2150) | H | H | H | H | 0(0.2) | −2 | 2MASS | iso | 10.77 |
| IRAS 06111−7020 | H | H | H | H | 0(0) | −2 | 2MASS | iso | 10.99 |
| IRAS 06259−4708 obj1 | H | H | H | H | 0(0.2) | 10.3 | 2MASS | a | 11.10 |
| IRAS 06259−4708 obj2 | cp | H | H | cp | 0.1(0.3) | 10.3 | 2MASS | a | ... |
| IRAS 06592−6313 | cp | H | H | cp | 0.1(0.4) | −2 | 2MASS | iso | 11.10 |
| IRAS 06593−7551 | H | H | H | H | 0(0.1) | −2 | 2MASS | iso | 10.07 |
| IRAS 07027−6011 | S2 | S2 | S2 | S2 | 0.9(0.8) | 50. | 2MASS | a | 11.41 |
| IRAS 07269−6811 | ... | ... | ... | ... | ... | 8.6 | 2MASS | b | 11.66 |
| IRAS 08007−6600 | | | | cp | 0.4(0.3) | −2 | 2MASS | iso | 11.52 |
| IRAS 08087+0347(NGC 2358) | | | | cp | 0.2(0.3) | −2 | 2MASS | iso | 10.47 |
| IRAS 08169+0448(NGC 2561) | ... | ... | ... | ... | ... | 100: | DSS | iso | 10.37 |
| IRAS 08225−6936 | H | H | H | H | 0(0.1) | −2 | 2MASS | iso | 10.52 |
| IRAS 08438−1510 | cp | H | S2 | cp: | 0.5(0.5) | −2 | 2MASS | iso | 10.75 |
| IRAS 08480−0254(MRK1414) | H | H | H | H | 0(0.1) | −2 | 2MASS | iso | 10.46 |
| IRAS 08511−1028 | H | H | H | H | 0(0.2) | −2 | 2MASS | iso | 10.88 |
| IRAS 08561+0629(NGC 2718) | H | H | H | H | 0(0.2) | −2 | 2MASS | iso | 10.48 |
| IRAS 08594+0829 | ... | ... | ... | ... | ... | −2 | 2MASS | iso | 10.0 |
| IRAS 09004−2031 | H | H | H | H | 0(0.2) | 7. | 2MASS | b | 10.39 |
| IRAS 09070+0722 | H | H | H | H | 0(0.2) | −2 | 2MASS | iso | 10.66 |
| IRAS 09143+0939 | ... | ... | ... | ... | ... | −2 | 2MASS | iso | 11.5 |
| IRAS 09248−1918 | cp | H | H | cp | 0.2(0.3) | −2 | 2MASS | iso | 10.70 |
| IRAS 09324−2142 | S2 | S2 | S2 | S2 | 0.8(0.8) | 16.3 | 2MASS | a | 10.47 |
| IRAS 09395+0454(NGC 2966) | H | H | H | H | 0(0.2) | 100: | DSS | iso | 10.37 |
| IRAS 09426−1928 | cp | H | H | cp | 0.4(0.3) | 29. | 2MASS | a | 10.52 |
| IRAS 09433−1531 | H | H | H | H | 0(0.1) | 5. | 2MASS | b | 10.75 |
| IRAS 09432−1405(NGC 2993) | H | H | H | H | 0(0.2) | 25. | 2MASS | a | 10.43 |
| IRAS 09521+0930(NGC 3049) | H | H | H | H | 0(0.1) | −2 | 2MASS | iso | 9.44 |
| IRAS 09591−1317 | ... | ... | ... | ... | ... | −2 | 2MASS | iso | 10.57 |
| IRAS 10036−0057 | cp | H | H | cp | 0.6(0.4) | 3.5 | 2MASS | b | 11.34 |
| IRAS 10042−2941(NGC 3125) obj1 | H | H | H | H | 0(0.2) | 0.6 | 2MASS | b | 9.22 |
| IRAS 10042−2941(NGC 3125) obj2 | H | H | H | H | 0(0.2) | 0.6 | 2MASS | b | 9.22 |
| IRAS 10057−3343 | cp | H | H | cp | 0.3(0.5) | −2 | 2MASS | iso | 11.13 |
| IRAS 10140−3318(IC2560) | S2 | S2 | S2 | S2 | 1(1) | −2 | 2MASS | iso | 10.20 |

**Table 3**
(Continued)

| Name | Spectral Type | | | | $D_{AGN}$ | *ns* | Reference | Morphology | $\log(L_{IR}/L_{\odot})$ |
|---|---|---|---|---|---|---|---|---|---|
| | [N II] | [S II] | [O I] | Adopt | | (kpc) | | Class | |
| (1) | (2) | (3) | (4) | (5) | (6) | (7) | (8) | (9) | (10) |
| IRAS 10219−2828 | ... | ... | ... | ... | ... | 7.6 | 2MASS | b | 11.17 |
| IRAS 10221−2317 | S2 | H | S2 | S2: | 0.5(0.5) | −2 | 2MASS | iso | 10.80 |
| IRAS 10295−1831 | S2 | H | S2 | S2: | 0.6(0.6) | −2 | 2MASS | iso | 11.30 |
| IRAS 10295−3435(NGC 3281) | S2 | S2 | S2 | S2 | 1(1) | −2 | 2MASS | iso | 10.69 |
| IRAS 10323−2819 | H | H | H | H | 0(0.3) | 6.8 | 2MASS | b | 10.23 |
| IRAS 11083−2813 | | | | S1 | 1(1) | −2 | 2MASS | iso | 11.00 |
| ∗IRAS 11095−0238 | ... | ... | ... | ... | ... | −1 | 2MASS | cde | 12.17 |
| IRAS 11100+0919(IC676) | H | H | H | H | 0(0.2) | −2 | 2MASS | iso | 9.50 |
| IRAS 11122−2327(NGC 3597) | H | H | H | H | 0(0.2) | −1 | 2MASS | cde | 10.81 |
| IRAS 11149+0449(NGC 3611) | H | H | H | H | 0(0.2) | 100: | DSS | iso | 9.77 |
| IRAS 11178+0351(NGC 3633) | ... | ... | ... | ... | ... | −2 | 2MASS | iso | 10.06 |
| IRAS 11186−0242 | ... | ... | ... | ... | ... | −2 | 2MASS | iso | 11.22 |
| IRAS 11264+0923 | ... | ... | ... | ... | ... | −2 | 2MASS | iso | 10.90 |
| IRAS 11273−0607 | ... | ... | ... | ... | ... | −2 | 2MASS | iso | 11.53 |
| IRAS 11316−0934(NGC 3732) | H | H | H | H | 0(0.2) | −2 | 2MASS | iso | 9.82 |
| IRAS 11365−3727(NGC 3783) | | | | S1 | 1(1) | −2 | 2MASS | iso | 10.29 |
| IRAS 11396+0036 | H | H | H | H | 0(0.2) | −1 | 2MASS | cde | 10.75 |
| IRAS 11409−1631 | H | H | H | H | 0(0) | 1.2 | 2MASS | b | 10.44 |
| IRAS 11430+0330(NGC 3849) | ... | ... | ... | ... | ... | −2 | 2MASS | iso | 10.80 |
| IRAS 11442−2738(NGC 3885) | ... | ... | ... | ... | ... | −2 | 2MASS | iso | 10.22 |
| IRAS 11514−2253(NGC 3955) | ... | ... | ... | ... | ... | −2 | 2MASS | iso | 9.77 |
| IRAS 12056+0309(NGC 4123) | H | H | H | H | 0(0.2) | −2 | 2MASS | iso | 9.73 |
| IRAS 12063−3625 | ... | ... | ... | ... | ... | −2 | 2MASS | iso | 10.39 |
| IRAS 12071−0444 | ... | ... | ... | ... | ... | −1 | 2MASS | cde | 12.29 |
| IRAS 12121−3513 | H | H | H | H | 0(0.2) | 61 | DSS | a | 10.57 |
| IRAS 12174−1706 | H | H | H | H | 0(0.1) | −2 | 2MASS | iso | 8.89 |
| IRAS 12193−4303 | ... | ... | ... | ... | ... | 4. | 2MASS | b | 11.10 |
| IRAS 12195−3312(NGC 4304) | H | H | H | H | 0(0.2) | −2 | 2MASS | iso | 10.32 |
| IRAS 12231+0050(NGC 4385) | cp | H | H | cp | 0.3(0.3) | −2 | 2MASS | iso | 10.04 |
| IRAS 12240+0414 (NGC 4412) | S2 | S2 | S2 | S2 | 0.5(0.6) | −2 | 2MASS | iso | 9.70 |
| IRAS 12243−0036 (NGC 4418) | ... | ... | ... | ... | ... | −2 | 2MASS | iso | 10.86 |
| IRAS 12246+0941(NGC 4424) | ... | ... | ... | ... | ... | −2 | 2MASS | iso | 8.33 |
| IRAS 12286−2600 | cp | H | H | cp | 0.1(0.2) | −2 | 2MASS | iso | 10.86 |
| IRAS 12329−3938(NGC 4507) | S2 | S2 | S2 | S2 | 1(0.9) | −2 | 2MASS | iso | 10.51 |
| IRAS 12370−0504(NGC 4593) | | | | S1 | 1(1) | −2 | 2MASS | iso | 10.11 |
| IRAS 12381−3628 (IC3639) | S2 | S2 | S2 | S2 | 1(1) | −2 | 2MASS | iso | 10.67 |
| IRAS 12398−0641 (NGC 4628) | ... | ... | ... | ... | ... | −2 | 2MASS | iso | 10.21 |
| IRAS 12456−0303(NGC 4691) | H | H | H | H | 0(0.1) | −2 | 2MASS | iso | 9.90 |
| IRAS 12465−1108 (NGC 4700) | H | H | H | H | 0(0) | −2 | 2MASS | iso | 9.43 |
| IRAS 12476+0751 | ... | ... | ... | ... | ... | −1 | 2MASS | cde | 11.37 |
| IRAS 12499−0930(MRK1337) | H | H | H | H | 0(0.2) | 39 | DSS | a | 10.11 |
| IRAS 12504−2711 | ... | ... | ... | ... | ... | −2 | 2MASS | iso | 10.49 |
| IRAS 12540−4251 | cp | H | S2 | cp: | 0.5(0.5) | −2 | 2MASS | iso | 10.41 |
| IRAS 12542−0815(NGC 4818) | cp | H | H | cp | 0.5(0.3) | −2 | 2MASS | iso | 10.04 |
| IRAS 12550−2929 | cp | H | H | cp | 0.2(0.3) | −2 | 2MASS | iso | 10.43 |
| IRAS 12596−1529 obj2 | cp | H | H | cp | 0.1(0.3) | | 2MASS | b | 10.93 |
| IRAS 12596−1529 obj3 | H | H | H | H | 0(0.1) | 1.2 | ke01 | b | ... |
| IRAS 13035−4008 | | | | S1 | 1(1) | −2 | 2MASS | iso | 10.85 |
| IRAS 13062−1514 (NGC 4984) | cp | H | H | cp | 0.2(0.4) | −2 | 2MASS | iso | 9.87 |
| IRAS 13067−0500(NGC 4990) | cp | H | H | cp | 0.4(0.3) | −2 | 2MASS | iso | 10.15 |
| IRAS 13081−4557 | H | H | H | H | 0(0.2) | −2 | 2MASS | iso | 10.10 |
| IRAS 13123−1541(NGC 5038) | cp | H | H | cp | 0.2(0.5) | 100: | DSS | iso | 10.29 |
| IRAS 13154−0002 | H | H | H | H | 0(0.2) | 36.8 | DSS | a | 11.18 |
| IRAS 13157+0635 | ... | ... | ... | ... | ... | 16.2 | 2MASS | a | 10.87 |
| IRAS 13167−1435(NGC 5073) | H | H | H | H | 0(0.2) | −2 | 2MASS | iso | 10.50 |
| IRAS 13183−1212(NGC 5097) | H | H | H | H | 0(0.1) | −2 | 2MASS | iso | 9.91 |
| IRAS 13197−1627 | H | H | H | H | 0(0.2) | 32. | 2MASS | a | 11.07 |
| IRAS 13197−3928 | H | H | H | H | 0(0.2) | −1 | 2MASS | cde | 11.09 |
| IRAS 13229−2934(NGC 5135) | S2 | S2 | S2 | S2 | 0.8(0.8) | −2 | 2MASS | iso | 11.16 |
| IRAS 13244−4240 | H | H | H | H | 0(0.2) | −1 | 2MASS | cde | 11.17 |
| IRAS 13286−3432(NGC 5188) | cp | H | H | cp | 0.1(0.3) | −2 | 2MASS | iso | 10.72 |
| IRAS 13303−1559 | H | H | H | H | 0(0.2) | −2 | 2MASS | iso | 11.00 |
| IRAS 13333−1700 | ... | ... | ... | ... | ... | −1 | 2MASS | cde | 11.58 |

**Table 3**
(Continued)

| Name | Spectral Type | | | | $D_{AGN}$ | *ns* | Reference | Morphology | $\log(L_{IR}/L_{\odot})$ |
|---|---|---|---|---|---|---|---|---|---|
| | [N II] | [S II] | [O I] | Adopt | | (kpc) | | Class | |
| (1) | (2) | (3) | (4) | (5) | (6) | (7) | (8) | (9) | (10) |
| IRAS 13336−0046 obj1 | cp | H | H | cp | 0.2(0.4) | 12.2 | 2MASS | a | 11.67 |
| IRAS 13336−0046 obj2 | ... | ... | ... | ... | ... | 12.2 | 2MASS | a | 11.67 |
| IRAS 13370−3123 | ... | ... | ... | ... | ... | −2 | 2MASS | iso | 9.05 |
| IRAS 13373+0105(NGC 5257) | ... | ... | ... | ... | ... | 32.7 | 2MASS | a | 11.43 |
| IRAS 13379+0501 | cp | H | H | cp | 0.1(0.3) | −2 | 2MASS | iso | 10.87 |
| IRAS 14002−4108(NGC 5408) | H | H | H | H | 0(0.2) | −2 | 2MASS | iso | 8.37 |
| IRAS 14036+0234 | ... | ... | ... | ... | ... | 18.6 | 2MASS | a | 11.12 |
| IRAS 14104−1350 | S2 | S2 | S2 | S2 | 0.5(0.6) | −1 | 2MASS | cde | 11.86 |
| IRAS 14106−0258(NGC 5506) | S2 | S2 | S2 | S2 | 1(0.9) | 26.2 | DSS | a | 10.28 |
| IRAS 14137−4444(IC4390) | ... | ... | ... | ... | ... | −2 | 2MASS | iso | 9.75 |
| IRAS 14150−0711(NGC 5534) | H | H | H | H | 0(0.2) | 4.5 | 2MASS | b | 10.22 |
| IRAS 14209−1306 | ... | ... | ... | ... | ... | −1 | 2MASS | cde | 10.78 |
| IRAS 14216−1632(NGC 5597) | ... | ... | ... | ... | ... | 100: | DSS | iso | 10.54 |
| IRAS 14294−4357(NGC 5643) | S2 | S2 | S2 | S2 | 1(1) | −2 | 2MASS | iso | 10.10 |
| IRAS 14299+0817(NGC 5665) | H | H | H | H | 0(0.1) | −2 | 2MASS | iso | 10.29 |
| IRAS 14309−1424 | S2 | S2 | S2 | S2 | 0.7(0.7) | 6.7 | 2MASS | b | 10.5 |
| IRAS 14353−0011 (NGC 5691) | H | H | H | H | 0(0.1) | −2 | 2MASS | iso | 9.85 |
| IRAS 14376−0004(NGC 5713) | cp | H | H | cp | 0.1(0.2) | −2 | 2MASS | iso | 10.61 |
| IRAS 14384−3742 | ... | ... | ... | ... | ... | −2 | 2MASS | iso | 11.36 |
| IRAS 14430−3728 | ... | ... | ... | ... | ... | −2 | 2MASS | iso | 10.77 |
| IRAS 14483+0519(NGC 5765) | S2 | S2 | S2 | S2 | 0.8(0.8) | 11.5 | 2MASS | a | 11.19 |
| IRAS 14515−1504 | ... | ... | ... | ... | ... | −2 | 2MASS | iso | 11.01 |
| IRAS 14575−2615 obj1 | H | S2 | S2 | S2: | ... (0.3) | 10.4 | DSS | a | 10.65 |
| IRAS 14575−2615 obj2 | H | H | H | H | 0(0.3) | 10.4 | DSS | a | 10.65 |
| IRAS 15028+0820 | ... | ... | ... | ... | ... | −1 | 2MASS | cde | 11.41 |
| IRAS 15065−1107(NGC 5861) | ... | ... | ... | ... | ... | 100: | DSS | iso | 10.29 |
| IRAS 15150−1724(NGC 5890) | ... | ... | ... | ... | ... | −2 | 2MASS | iso | 9.82 |
| IRAS 15172−3115 | H | H | H | H | 0(0.2) | −1 | 2MASS | cde | 10.81 |
| IRAS 15188−0711 | ... | ... | ... | ... | ... | 30. | 2MASS | a | 9.87 |
| IRAS 15229+0511 | ... | ... | ... | ... | ... | 84.5 | DSS | a | 11.18 |
| IRAS 15257+0302 | H | H | H | H | 0(0.1) | −2 | 2MASS | iso | 11.25 |
| IRAS 15268−7757 | H | H | H | H | 0(0.2) | −2 | 2MASS | iso | 9.86 |
| IRAS 15320−2601 | ... | ... | ... | ... | ... | −1 | 2MASS | cde | 11.97 |
| IRAS 15361−0313 | ... | ... | ... | ... | ... | −2 | 2MASS | iso | 10.99 |
| IRAS 15437+0234(NGC 5990) obj1 | S2 | S2 | S2 | S2 | 0.6(0.7) | 33.3 | 2MASS | a | 10.53 |
| IRAS 15437+0234(NGC 5990) obj2 | S2 | S2 | S2 | S2 | 0.6(0.7) | 33.3 | 2MASS | a | 10.53 |
| IRAS 15456−1336(NGC 5995) | | | | S1 | 1(1) | −2 | 2MASS | iso | 11.47 |
| ∗IRAS 15462−0450 | ... | ... | ... | ... | ... | −1 | 2MASS | cde | 12.37 |
| IRAS 16235+0301 | ... | ... | ... | ... | ... | −2 | 2MASS | iso | 9.58 |
| IRAS 16399−0937 obj1 | cp | H | H | cp | 0.2(0.2) | 3.5 | DSS | b | 11.07 |
| IRAS 16399−0937 obj2 | L | L | L | L | 0.7(0.7) | 3.5 | DSS | b | ... |
| IRAS 16487−0222 | ... | ... | ... | ... | ... | −2 | 2MASS | iso | 11.35 |
| IRAS 16504+0228(NGC 6240) | L | L | L | L | 0.8(0.7) | 0.74 | tec00 | b | 11.83 |
| IRAS 17138−1017 | cp | H | H | cp | 0.2(0.3) | −1 | 2MASS | cde | 11.50 |
| ∗IRAS 17324−6855 | H | H | H | H | 0(0.2) | 3.6 | 2MASS | b | 12.15 |
| IRAS 17467+0807 | H | H | H | H | 0(0.2) | −2 | 2MASS | iso | 10.77 |
| IRAS 18078−5815 | cp | H | H | cp | 0.4(0.3) | −2 | 2MASS | iso | 10.13 |
| IRAS 18093−5744 obj1 | H | H | H | H | 0(0.2) | 8.7 | 2MASS | b | 10.68 |
| IRAS 18093−5744 obj2 | H | H | H | H | 0(0.2) | 8.7 | 2MASS | b | 10.68 |
| IRAS 18097−6006 | cp | H | H | cp | 0.2(0.3) | −2 | 2MASS | iso | 10.89 |
| IRAS 18325−5926 | S2 | H | S2 | S2: | 0.8(0.7) | −2 | 2MASS | iso | 11.10 |
| IRAS 18429−6312(IC4769) | S2 | S2 | S2 | S2 | 1(1) | 24.8 | DSS | a | 10.73 |
| IRAS 18432−6024 | ... | ... | ... | ... | ... | 3.8 | 2MASS | b | 11.48 |
| IRAS 18515−5347(NGC 6708) | H | H | H | H | 0(0) | −2 | 2MASS | iso | 10.17 |
| IRAS 19184−6822 | H | H | H | H | 0(0.2) | −2 | 2MASS | iso | 10.64 |
| IRAS 19254−7245 | | | | S1 | 1(1) | 9.3 | 2MASS | b | 11.99 |
| IRAS 19335−2011 obj1 | H | H | H | H | 0(0.2) | 7.6 | 2MASS | b | 11.46 |
| IRAS 19335−2011 obj2 | H | H | H | H | 0(0.2) | 7.6 | 2MASS | b | 11.46 |
| IRAS 19393−5846(NGC 6810) | cp | H | H | cp | 0.4(0.3) | −2 | 2MASS | iso | 10.6 |
| IRAS 19412−3305 | S2 | S2 | S2 | S2 | 0.6(0.7) | −2 | 2MASS | iso | 11.16 |
| IRAS 19466−3649 | ... | ... | ... | ... | ... | 15.2 | 2MASS | a | 10.62 |
| IRAS 19543−3804 | S2 | S2 | S2 | S2 | 1(1) | −2 | 2MASS | iso | 11.07 |
| IRAS 19594−2021 | ... | ... | ... | ... | ... | −2 | 2MASS | iso | 10.81 |

**Table 3**
(Continued)

| Name | Spectral Type | | | | $D_{AGN}$ | $ns$ | Reference | Morphology | $\log(L_{IR}/L_{\odot})$ |
|---|---|---|---|---|---|---|---|---|---|
| | [N II] | [S II] | [O I] | Adopt | | (kpc) | | Class | |
| (1) | (2) | (3) | (4) | (5) | (6) | (7) | (8) | (9) | (10) |
| ∗IRAS 20046−0623 | cp | L | S2 | cp: | 0.5(0.3) | 21.5 | DSS | a | 12.08 |
| IRAS 20082+0058 | cp | H | H | cp | 0.3(0.5) | 57.4 | DSS | a | 10.97 |
| IRAS 20104−4430 | H | H | H | H | 0(0.2) | −2 | 2MASS | iso | 10.81 |
| IRAS 20114−5803(IC4980) | S2 | S2 | S2 | S2 | 1(1) | −2 | 2MASS | iso | 10.52 |
| IRAS 20122−0955 | ... | ... | ... | ... | ... | −1 | 2MASS | cde | 11.52 |
| IRAS 20178−0052 | cp | H | H | cp | 0.2(0.3) | 48.8 | DSS | a | 10.77 |
| IRAS 20205−4409(IC4946) | cp | H | H | cp | 0.1(0.3) | −2 | 2MASS | iso | 10.34 |
| IRAS 20244−5151 | cp | H | H | cp | 0.4(0.3) | −2 | 2MASS | iso | 10.75 |
| IRAS 20272−4738(NGC 6918) | cp | H | H | cp | 0.1(0.3) | −2 | 2MASS | iso | 10.18 |
| IRAS 20273−1523 | H | H | H | H | 0(0.2) | −2 | 2MASS | iso | 10.39 |
| IRAS 20332+0805 | cp | H | H | cp | 0.1(0.3) | −2 | 2MASS | iso | 11.03 |
| IRAS 20481−5715(IC5063) | S2 | S2 | S2 | S2 | 1(1) | −2 | 2MASS | iso | 10.76 |
| IRAS 20551−4250 | cp | H | H | cp | 0.4(0.2) | −1 | 2MASS | cde | 11.97 |
| IRAS 21023−4258 | H | H | H | H | 0(0.2) | −2 | 2MASS | iso | 10.01 |
| IRAS 21052+0340 obj1 | cp | H | H | cp | 0.3(0.2) | 34. | 2MASS | a | 11.06 |
| IRAS 21052+0340 obj2 | cp | H | H | cp | 0.3(0.2) | 34. | 2MASS | a | 11.06 |
| IRAS 21116+0158(IC368) | S2 | S2 | S2 | S2 | 0.9(1) | 100: | DSS | iso | 10.56 |
| IRAS 21330−3846 | H | H | H | H | 0(0.2) | 4. | 2MASS | b | 11.05 |
| IRAS 21497−0824 | S2 | S2 | S2 | S2 | 1(1) | −2 | 2MASS | iso | 11.26 |
| IRAS 21504−0628 | cp | H | L | cp: | 0.5(0.3) | −1 | 2MASS | cde | 11.92 |
| IRAS 21522−4717 | H | H | H | H | 0(0.1) | −2 | 2MASS | iso | 10.73 |
| IRAS 22007+0019(NGC 7189) | S2 | S2 | S2 | S2 | 0.6(0.7) | −2 | 2MASS | iso | 11.18 |
| IRAS 22045+0959(NGC 7212) | S2 | S2 | S2 | S2 | 1(1) | 7. | 2MASS | b | 11.09 |
| IRAS 22072−3620(IC5169) | cp | H | H | cp | 0.4(0.5) | −2 | 2MASS | iso | 10.28 |
| IRAS 22115−3013 | H | H | H | H | 0(0.1) | −2 | 2MASS | iso | 10.6 |
| IRAS 22127−4605(NGC 7233) | H | H | H | H | 0(0.1) | 13.1 | 2MASS | a | 10.01 |
| IRAS 22132−3705(IC5183) | ... | ... | ... | ... | ... | −2 | 2MASS | iso | 11.13 |
| IRAS 22225−3136 | ... | ... | ... | ... | ... | 4.9 | 2MASS | b | 11.16 |
| IRAS 22287−1917 | cp | H | H | cp | 0.5(0.5) | −2 | 2MASS | iso | 11.26 |
| IRAS 22397−3726 | cp | H | S2 | cp: | 0.5(0.5) | −2 | 2MASS | iso | 10.99 |
| IRAS 22467−4906 | S2 | H | S2 | S2: | 0.5(0.5) | −1 | 2MASS | cde | 11.70 |
| IRAS 23007+0836(NGC 7469) | | | | S1 | 1(1) | 25.1 | 2MASS | a | 11.58 |
| IRAS 23011+0046 | ... | ... | ... | ... | ... | −2 | 2MASS | iso | 11.31 |
| IRAS 23023−4322(NGC 7476) | H | H | H | H | 0(0.2) | −2 | 2MASS | iso | 10.19 |
| IRAS 23050+0359 | cp | H | H | cp | 0.2(0.2) | −1 | 2MASS | cde | 11.61 |
| IRAS 23069−4341(NGC 7496) | H | H | H | H | 0(0.2) | −2 | 2MASS | iso | 10.13 |
| IRAS 23128−5919 | ... | ... | ... | ... | ... | 4.1 | 2MASS | b | 11.95 |
| IRAS 23134−4251(NGC 7552) | H | H | H | H | 0(0.2) | −2 | 2MASS | iso | 10.98 |
| IRAS 23156−4238(NGC 7582) | H | H | H | H | 0(0.1) | 71.7 | DSS | a | 10.79 |
| IRAS 23157−0441(NGC 7592) obj1 | S2 | S2 | S2 | S2 | 0.6(0.6) | 7. | DSS | b | 11.34 |
| IRAS 23157−0441(NGC 7592) obj2 | H | H | H | H | 0(0.1) | 7. | DSS | b | ... |
| IRAS 23192−4245(NGC 7632) | ... | ... | ... | ... | ... | −2 | 2MASS | iso | 11.43 |
| IRAS 23201+0805 | S2 | S2 | S2 | S2 | 0.8(0.8) | −2 | 2MASS | iso | 11.33 |
| IRAS 23204+0601 | ... | ... | ... | ... | ... | −1 | 2MASS | cde | 11.80 |
| IRAS 23215−1208 | ... | ... | ... | ... | ... | −2 | 2MASS | iso | 10.96 |
| IRAS 23254+0830(NGC 7674) | S2 | S2 | S2 | S2 | 1(1) | 17.4 | 2MASS | a | 11.52 |
| IRAS 23262+0314(NGC 7679) | | | | S1 | 1(1) | −2 | 2MASS | iso | 11.07 |
| IRAS 23336+0152(NGC 7714) | H | H | H | H | 0(0.3) | 20.5 | 2MASS | a | 10.72 |
| IRAS 23414+0014(NGC 7738) | cp | H | H | cp | 0.3(0.5) | −2 | 2MASS | iso | 11.08 |

**Notes.** We only list the spectral type results for galaxies having available line ratios with S/N $> 3\sigma$ in all three BPT diagrams. The projected radius used for searching companions is ∼100 kpc. Columns 1–6: the same as Table 2. Column 7: projected nuclear separation. −1: single nucleus with tidal features; −2: isolated systems ":": lower limit; "m": multiple (more than two) interacting objects. Column 8: references used to obtain projected separation. 2MASS: 2MASS images ($K_s$ band); DSS: DSS images; cb96: Clements & Baker (1996); hv95: Heisler & Vader (1995); vva68: Vorontsov-Velyaminov & Arhipova (1968); ke01: Kewley et al. (2001b); tec00: Tecza et al. (2000). Column 9: adopted morphology class, a: wide binary; b: close binary; cde: single merger (either diffuse merger, compact merger, or old merger); iso: isolated system; m: multiple mergers. Symbols: H = star-forming galaxies, L = LINERs, S2 = Seyfert 2 galaxies, S1 = Seyfert 1 galaxies, cp = starburst–AGN composite galaxies. Column 10: $\log(L_{IR}/L_{\odot})$, data from Kewley et al. (2001b).

"diffuse," "compact," and "old" merger stages as one "single-merger" stage so that each class contains at least 10 galaxies.

The final morphological classes for the SW01 and BGS samples are as follows.

1. Wide binary: "binary systems" with projected separation $ns > 10$ kpc.
2. Close binary: "binary systems" with projected separation $ns < 10$ kpc.

**Table 4**
Spectral Classification as a Function of $L_{IR}$ for the 1 Jy ULIRG + BGS Samples

| Spectral Type | $\log(L_{IR}/L_{\odot})$ | | | |
|---|---|---|---|---|
| | <11 | 11–11.99 | 12–12.29 | 12.3–12.8 |
| New classification, excluding double-nuclei objects, 3-of-3 criterion | | | | |
| Total number | 22 | 51 | 69 | 31 |
| Starburst | 8(36.4%) | 12(23.5%) | 3(4.3%) | 1(3.2%) |
| Starburst–AGN composite | 8(36.4%) | 19(37.3%) | 33(47.8%) | 12(38.7%) |
| Seyfert 2 | 1(4.5%) | 7(13.7%) | 13(18.8%) | 8(25.8%) |
| Seyfert 1 | 0(0%) | 1(2%) | 2(2.9%) | 8(25.8%) |
| LINER | 2(9.1%) | 3(5.9%) | 3(4.3%) | 0(0%) |
| Ambiguous | 3(13.6%) | 9(17.6%) | 15(21.7%) | 2(6.5%) |
| New classification, excluding double-nuclei objects, 2-of-3 criterion | | | | |
| Total number | 22 | 51 | 69 | 31 |
| Starburst | 10(45.5%) | 12(23.5%) | 7(10.2%) | 1(3.2%) |
| Starburst–AGN composite | 8(36.3%) | 19(37.3%) | 33(47.8%) | 12(38.7%) |
| Seyfert 2 | 2(9.1%) | 16(31.3%) | 24(34.8%) | 10(32.3%) |
| Seyfert 1 | 0(0%) | 1(2%) | 2(2.9%) | 8(25.8%) |
| LINER | 2(9.1%) | 3(5.9%) | 3(4.3%) | 0(0%) |

**Notes.** Number of galaxies and their fraction (shown in brackets) in each spectral type class. Top rows are results from the 3-of-3 criterion (not including galaxies with double nuclei); bottom rows are results from the 2-of-3 criterion (not including galaxies with double nuclei).

3. Single merger: single systems ($ns \sim 0$) with tidal features or distorted nuclei recognizable in available images.
4. Isolated system: systems that have no obvious signs of merging or interaction, within the 100 kpc image search radius.

There may be some overlap in the "isolated" and "single-merger" groups, as it is impossible to distinguish whether a galaxy is truly "isolated" or is simply at the end of the merging stage where all the tidal features disappear (or are too faint to be observed). For example, there are seven single-nucleus ULIRGs in the SW01 sample that do not show obvious signs of merging in available NED images. However, 1 Jy *R*-band images show remnant signs of tidal activity for three of the single-nuclei galaxies.

Besides the uncertainty in distinguishing the "isolated systems" from "single mergers," there are some classical drawbacks in using projected separation as a tracer for merger processes.

1. Projection effects may randomize the results. However, for a large sample, projection effects should be statistically unimportant; on average, interacting systems with $ns \lesssim$ few kpc are likely to be at a later stage in the merger process than systems with $ns \gtrsim$ a few 10 kpc.
2. Merger models such as Barnes & Hernquist (1992, 1996) show that *ns* is not necessarily a linear function of time: the projected separation decreases in a period of close contact ("first-pass") and then increases again before the nuclei finally merge.
3. Projected nuclear separation cannot trace merger progress in multiple mergers of more than two galaxies unless the time between current mergers and that of the former mergers is sufficiently large to enable any merger-induced star formation and AGN activity to subside (Borne et al. 2000). This issue may be a potential problem for the SW01 sample, in which some galaxies are in the Hickson Compact Groups (Garcia 1993). In these groups, the IR emission may be triggered by the weak interaction between the group members. For the 1 Jy sample, multiple mergers are not a major concern because deep images indicate that only 5/118 (<5%) are *possible* multiple mergers (Veilleux et al. 2002).

With these caveats in mind, we calculate the projected separation between paired galaxies in our samples using 2MASS $K_s$-band images for the BGS and SW01 samples, and the Veilleux et al. (2002) $K_s$-band projected separation measurements for the 1 Jy sample.

## 3. RESULTS

### 3.1. Spectral Type as a Function of IR Luminosity

Our samples span different luminosity ranges and have different IR color-selection criteria. To examine how spectral type changes with IR luminosity, we combine the 1 Jy ULIRG sample with the BGS sample to cover a broad IR luminosity range and to facilitate comparisons with the classical Veilleux et al. (1999) result. We consider the SW01 sample separately in this case because the warm color criterion of the SW01 sample may affect how the spectral type changes with IR luminosity.

Figure 4 shows the optical spectral type as a function of $L_{IR}$ for the combined 1 Jy and BGS samples. The results are also tabulated in Table 4. It is obvious from this figure that LINERs are rare compared with other spectral classes in our IR-luminous samples, with only 3% LINERs in the 1 Jy sample and 7% in the BGS sample. The 1 Jy ULIRGs sample may lack LINERs because this sample is selected at larger redshifts than the SDSS. Ke06 showed that the fraction of LINERs in the SDSS falls at $z > 0.1$ due to incompleteness. The lack of LINERs in SW01 may be at least partly caused by the warm selection criterion, as the "warm" criterion selects against LINERs (Kewley et al. 2001b).

We find few IR-luminous LINERs found in our samples. A majority (72/79) of the objects previously classified as LINERs are classified as composite galaxies and Seyfert 2s using the Ke06 SDSS-based classification scheme. LINERs in the SDSS-based classification scheme contain an older stellar population and an AGN with a lower accretion rate than Seyfert 2 galaxies. The lack of such LINERs in IR samples indicates that (a) bona

**Table 5**
Spectral Classification as a Function of $L_{IR}$ for the SW01 Sample

| Spectral Type | log ($L_{IR}/L_{\odot}$) | | | |
|---|---|---|---|---|
| | 8.0–10.19 | 10.2–10.69 | 10.7–11.09 | 11.1–12.2 |
| New classification, excluding double-nuclei objects, 3-of-3 criterion | | | | |
| Total number | 37 | 49 | 49 | 41 |
| Starburst (H II region) | 25(67.6%) | 25(51.0%) | 15(30.6%) | 5(12.2%) |
| Starburst–AGN composite | 7(18.9%) | 13(26.5%) | 19(38.8%) | 15(36.5%) |
| Seyfert 2 | 4(10.8%) | 8(16.3%) | 7(14.3%) | 14(34.2%) |
| Seyfert 1 | 0(0%) | 2(4.1%) | 3(6.1%) | 5(12.2%) |
| LINER | 1(2.7%) | 0(0%) | 1(2.0%) | 0(0.0%) |
| Ambiguous | 0(0%) | 1(2.1%) | 4(8.2%) | 2(4.9%) |

**Notes.** Since the fraction of ambiguous galaxies in SW01 is small, we only list the stringent 3-of-3 criterion results here. Detail classification for a specific ambiguous galaxy can be found in Table 3.

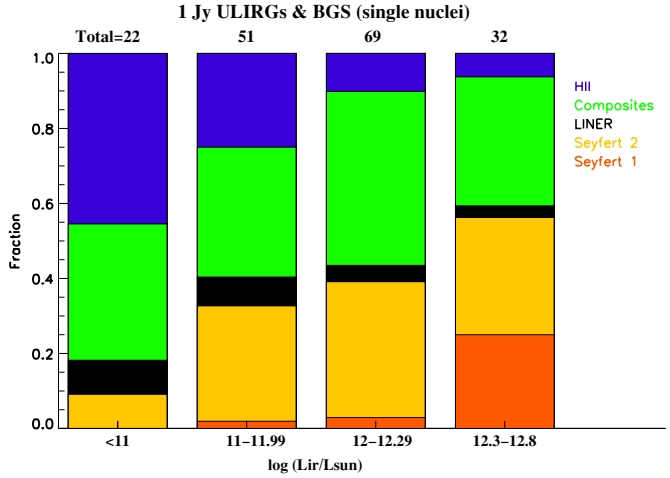


**Figure 4.** Spectral type (2-of-3 criterion) as a function of $L_{IR}$ for the 1 Jy ULIRG sample (Veilleux et al. 1999) and the LIRGs in the BGS sample (Veilleux et al. 1995). Similar to Veilleux et al. (1999), double-nucleus objects are excluded in this figure. The number of galaxies contained in each bin is marked on top of the histogram. The luminosity bins are labeled at the bottom. Throughout this paper we will always use gray for ambiguous, blue for H II-region galaxies, green for composites, black for LINERs, yellow for Seyfert 2 galaxies, and orange for Seyfert 1 galaxies, unless otherwise specified. The result of applying the stringent 3-of-3 criterion is presented in Appendix B.

(A color version of this figure is available in the online journal.)

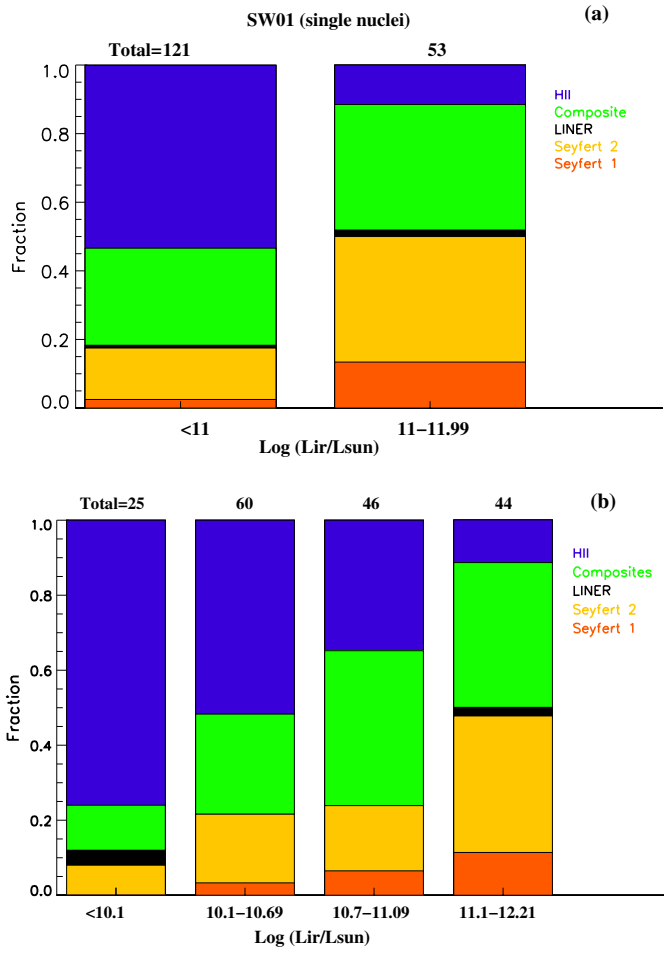


**Figure 5.** Optical classification results as a function of $L_{IR}$ for the SW01 sample. The SW01 sample is dominated by moderate IR-luminosity $L_{IR} < 10^{11}\ L_{\odot}$ sources, with ~25% LIRGs, and very few ULIRGs (<2% = 3 objects). For comparison with Figure 4, panel (a) divides the SW01 sample into the same two lower luminosity bins (only three SW01 objects have $L_{IR} > 10^{12}\ L_{\odot}$ in the bin $12 < \log(L_{IR}/L_{\odot}) < 12.21$). Panel (b) provides a finer grouping into four $L_{IR}$ bins to gain more resolution. The sub-bins are chosen in such a way that each bin contains at least 20 galaxies.

(A color version of this figure is available in the online journal.)

fide IR-luminous LINERs are quite rare—only 3/108 in the 1 Jy ULIRG sample and 5/97 in the BGS samples, and (b) in most cases, LINERs do not contain the intense star formation and/or the strong dust-reprocessed AGN emission responsible for the IR luminosities seen in U/LIRGs. We discuss the rare IR-selected LINERs in more detail in Section 4.1.

Interestingly, we find that Seyfert 1 galaxies favor higher $L_{IR}$, consistent with previous studies suggesting that Seyfert 2 galaxies have weaker mid-IR luminosities than Seyfert 1 galaxies (Heckman 1995; Maiolino et al. 1995; Giuricin et al. 1995; however, see Bonatto & Pastoriza 1997; Haas et al. 2007). However, because the 1 Jy ULIRG + BGS samples only contain a total of 11 Seyfert 1 galaxies, a larger number of IR-luminous Seyfert 1s is required to determine the significance of this result.

The spectral type as a function of $L_{IR}$ for the SW01 sample is shown in Figure 5 and Table 5. Because the SW01 sample covers a lower IR luminosity range, the SW01 sample is intended to extend the 1 Jy ULIRG and BGS samples to lower luminosities, rather than to serve as a comparison sample. Nevertheless, in panel (a) of Figure 5, the $L_{IR}$ bins are chosen to be the same as the first two bins of Figure 4 to facilitate comparisons between the warm (SW01) and non-warm (BGS and 1 Jy ULIRG) samples over the $L_{IR}$ range where all samples are well defined.

Since our samples contain a large number of objects with $L_{IR}/L_{\odot} < 10^{10}$, $L_{IR}$ is divided into sub-bins in panel (b) to

**Table 6**
Spectral Type as a Function of Morphology for the 1 Jy ULIRG Sample

| Spectral Type | Morphology Group[a] | | | | |
|---|---|---|---|---|---|
| | Wide Binary | Close Binary | Diffuse Merger | Compact Merger | Old Merger |
| Total number | 17 | 29 | 15 | 30 | 11 |
| Starburst | 2(11.8% ± 8.3%) | 5(17.2% ± 7.7%) | 0(0% ± 0%) | 0(0% ± 0%) | 0(0% ± 0%) |
| Starburst–AGN composite | 8(47% ± 16.7%) | 16(55.2% ± 13.7%) | 12(80.0% ± 23.1%) | 11(36.6% ± 11.1%) | 4(36.4% ± 18.1%) |
| LINER | 0(0% ± 0%) | 2(6.9% ± 4.9%) | 1(6.7% ± 6.7%) | 0(0% ± 0%) | 0(0% ± 0%) |
| Seyfert 2 | 7(41.2% ± 15.6%) | 6(20.7% ± 8.4%) | 2(13.3% ± 9.4%) | 11(36.7% ± 11.1%) | 5(45.4% ± 20.3%) |
| Seyfert 1 | 0(0% ± 0%) | 0(0% ± 0%) | 0(0% ± 0%) | 8(26.7% ± 9.4%) | 2(18.2% ± 12.9%) |

**Notes.**
[a] The one isolated object and five possible triple-system objects are not included here. The mean and standard error of the fractions are shown in the brackets.

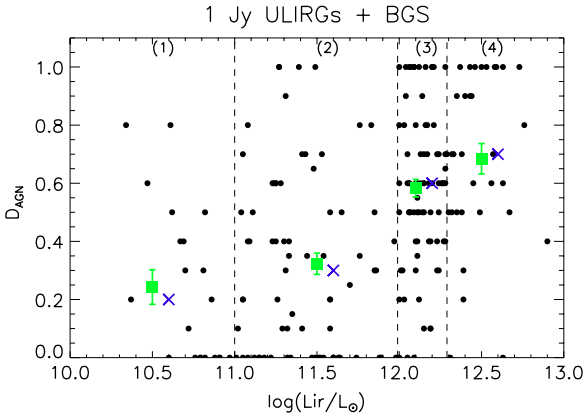


**Figure 6.** $D_{AGN}$ as a function of $L_{IR}$ for the 1 Jy ULIRG + BGS sample. The mean, median, and standard error of the mean for the same four IR luminosity bins used in Figure 4 are plotted in green. Blue crosses give the median values. The probability that the $D_{AGN}$ distribution in consecutive bin pairs is drawn from the same parent population is given in Section 3.2. The rise in $D_{AGN}$ from luminosity bin (2) to (3) and bin (3) to (4) is significant at the 99% and 90% confidence levels, respectively.

(A color version of this figure is available in the online journal.)

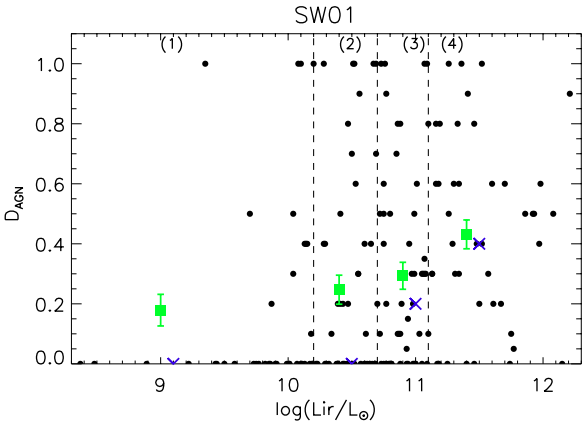


**Figure 7.** $D_{AGN}$ as a function of $L_{IR}$ for the SW01 sample. The mean, median, and standard error of the mean for the same four IR luminosity bins used in Figure 5 panel (b) are plotted in green. Blue crosses are the median values. The probability that the $D_{AGN}$ distribution in consecutive bin pairs is drawn from the same parent population is given in Section 3.2. The rise in $D_{AGN}$ from luminosity bin (3) to (4) is significant at the 98% confidence level.

(A color version of this figure is available in the online journal.)

improve resolution. Bin sizes are chosen to ensure that each bin contains at least 20 galaxies. In the SW01 sample, the AGN fraction increases and the fraction of starbursts decreases as $L_{IR}$ becomes larger, similar to the trend in the 1 Jy ULIRG + BGS samples. As shown in panel (b) of Figure 5, the lowest luminosity bin ($L_{IR}/L_{\odot} < 10^{10}$) has the largest fraction of star-forming galaxies.

### 3.2. $D_{AGN}$ as a Function of $L_{IR}$

Spectral types only reflect the galaxy's general position on the BPT diagrams. To investigate the relative contribution from an AGN as a function of IR luminosity, we show in Figures 6 and 7 $D_{AGN}$ as a function of $L_{IR}$ for the combined 1 Jy ULIRG + BGS sample, and the SW01 sample, respectively. The mean, median, and standard errors for $D_{AGN}$ are calculated for the same four luminosity ranges as used in Figures 4 and 5(b), for the combined 1 Jy ULIRG + BGS sample and the SW01 sample, respectively. To test whether the distribution of $D_{AGN}$ in each $L_{IR}$ bin can be drawn randomly from the same parent population, we perform the two-sample Kolmogorov–Smirnov (K-S) test to each pair of neighboring $L_{IR}$ bins. For the $L_{IR}$ bin pairs (1-2), (2-3), (3-4) in Figure 6, the K-S test gives a probability $P_{null} =$ 0.08, 3.98E−6, and 0.16 that the distributions are drawn from the same parent population, indicating a statistically significant change in the $D_{AGN}$ distribution at the 90% confidence level between $10^{10} < L_{IR}/L_{\odot} < 10^{12.3}$ for the 1 Jy ULIRG + BGS sample.

For the SW01 $L_{IR}$ bin pairs (1-2), (2-3), (3-4) in Figure 7, the K-S test gives a probability $P_{null} = 0.48$, 0.28, and 0.02 that the distributions are drawn from the same parent population, indicating a statistically significant change in the $D_{AGN}$ distribution at the 98% confidence level between $10^{10.7} < L_{IR}/L_{\odot} < 10^{12.3}$. The rise in $D_{AGN}$ at lower luminosities is not statistically significant for the SW01 sample.

We conclude that the rise of $D_{AGN}$ with $L_{IR}$ is significant for all three samples at $L_{IR}/L_{\odot} > 10^{11.0}$. Previous studies indicate that the fraction of AGN increases at large $L_{IR}$ (e.g., Armus et al. 1990; Veilleux et al. 1995; Goto 2005). Figures 6 and 7 confirm these results.

### 3.3. Spectral Type as a Function of Morphology/Merger Stage

Following the morphological definitions in Section 2.4, in Figure 8, and Table 6 we give the spectral type as a function of merging stage for the 1 Jy ULIRG sample. The dashed line indicates the uncertainty in classification associated with the double-nuclei galaxies that have differing classifications for each nucleus. These galaxies are discussed in more detail in Appendix C.

The key significant features in Figure 8 are as follows.

1. The fraction of starburst–AGN composite galaxies reaches a peak at the diffuse merger stage, indicating that both

**Table 7**
Spectral Type as a Function of Morphology for the LIRGs in the BGS Sample

| Spectral Type | Morphology Group[a] | | | |
|---|---|---|---|---|
| | Wide Binary | Close Binary | Single Merger | Isolated |
| Total number | 20 | 13 | 9 | 35 |
| Starburst | 8(40.0%) | 6(46.1%) | 4(44.5%) | 12(34.3%) |
| Starburst–AGN composite | 9(45.0%) | 5(38.5%) | 3(33.3%) | 15(42.9%) |
| LINER | 0(0%) | 1(7.7%) | 1(11.1%) | 3(8.6%) |
| Seyfert 2 | 2(10.0%) | 1(7.7%) | 1(11.1%) | 5(14.2%) |
| Seyfert 1 | 1(5.0%) | 0(0%) | 0(0%) | 0(0%) |

**Notes.** Only 77 objects with both available spectral type and morphology classification are included.
[a] Wide binary ($ns > 10$ kpc); close binary ($ns < 10$ kpc); single merger: merger in the final merging stage where the two nuclei have merged into a single one; isolated non-merging systems.

**Table 8**
Spectral Type as a Function of Morphology for the SW01 Sample

| Spectral Type | Morphology Group[a] | | | |
|---|---|---|---|---|
| | Wide Binary | Close Binary | Single Merger | Isolated |
| Total number | 41 | 24 | 18 | 124 |
| Starburst (H II region) | 15(36.6%) | 14(58.4%) | 5(33.3%) | 55(46.2%) |
| Starburst–AGN composite | 14(34.2%) | 5(20.8%) | 5(33.3%) | 37(31.1%) |
| LINER | 0(0%) | 2(8.3%) | 0(0%) | 1(0.8%) |
| Seyfert 2 | 9(21.9%) | 2(8.3%) | 5(33.3%) | 22(18.5%) |
| Seyfert 1 | 3(7.3%) | 1(4.2%) | 0(0%) | 4(3.4%) |

**Notes.** Only 207 objects with both available spectral type and morphology classification are included.
[a] Wide binary ($ns > 10$ kpc); close binary ($ns < 10$ kpc); single merger: merger in the final merging stage where the two nuclei have merged into a single one; isolated: non-merging systems.

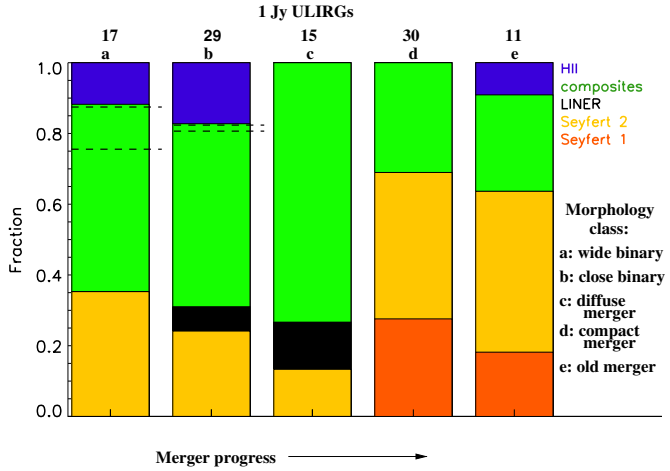


**Figure 8.** Optical spectroscopic classification as a function of merger morphology for the 1 Jy ULIRG sample. The merger progresses from left to right: (a) wide binary, (b) close binary, (c) diffuse merger, (d) compact merger, and (e) old merger. No "isolated" class is defined for the 1 Jy morphology class since there is only one isolated object in this sample. The number of galaxies in each morphology class is marked on top of each bin, and is given in Table 6. The fraction of composite galaxies reaches a peak at the diffuse merger stage. The fraction of AGN-dominated (Seyfert 2 and Seyfert 1) rises at later merger stages (compact and old merger). Dashed lines give the range of uncertainty in the fraction of H II and composites associated with the double-nuclei galaxies with different spectral types for each nucleus (see Appendix C).

(A color version of this figure is available in the online journal.)

merger-induced starburst activity, and AGN fueling contribute to the total energy budget at the diffuse merger stage.

2. The fraction of starburst–AGN composite galaxies falls sharply at the later merger stages (compact and old merger), giving rise to a larger portion of Seyfert galaxies rises in these later merger stages. We suggest that starburst–AGN composite galaxies evolve into Seyferts as merger-induced starburst activity subsides.

Figure 8 also shows potentially interesting trends that are limited by small numbers for the 1 Jy ULIRG sample.

1. The fraction of Seyfert galaxies appears to decrease ($41\% \pm 16\%$ compared to $13\% \pm 9\%$) between the wide binary stage (stage a) to the diffuse merger stage (stage c).
2. Seyfert 1 galaxies only occur at the later merger stages (d and e in Figure 8).

A larger sample of ULIRGs is required to verify these two trends.

We show the spectral type as a function of merger morphology for the BGS and SW01 samples in Figures 9 and 10, respectively. The results are listed in Tables 7 and 8. Clearly, for objects with $L_{IR}$ lower than that of ULIRGs, there is no strong change in spectral classification as a function of merger progress. However, the BGS and SW01 samples do not contain a sufficient number of galaxies in the single-merger stage that have deep enough images to allow separation into diffuse, compact, and old merger stages where the largest changes in spectral class occur for ULIRGs. The fraction of merging galaxies in the SW01 and BGS samples is 45% and 54%, respectively, compared with 99% for the 1 Jy ULIRG sample. In addition, most of the merging systems in the SW01 and BGS samples are in the earlier, binary stages rather than the advanced single-merger stages in the 1 Jy ULIRG sample (11% in the SW01 sample, and 12% in the BGS sample versus 50% in the 1 Jy ULIRG sample). If we combine objects in the 1 Jy ULIRG sample which have diffuse, compact, and old merger types into one single-merger class (Figure 11), the changes seen in Figure 10 disappear. These results highlight the need for sensitive *K*- and *B*-band imaging to distinguish

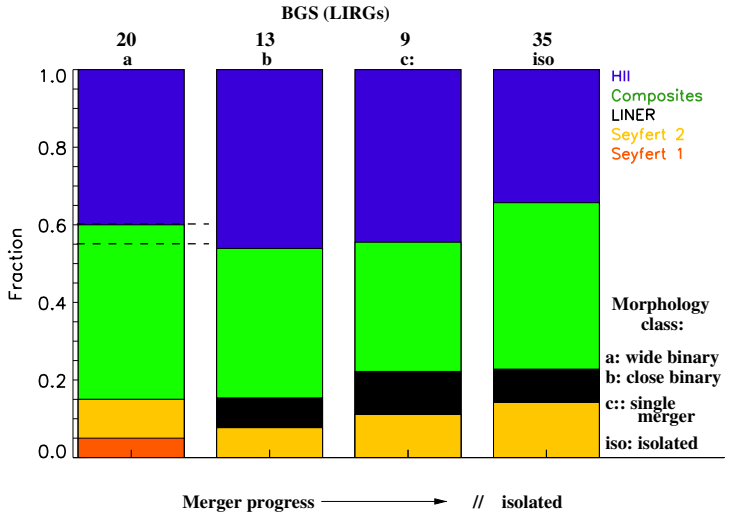


**Figure 9.** Spectral type as a function of morphology for the LIRGs in the BGS sample. The merger progresses from left to right: (a) wide binary, (b) close binary, (c) single-merger, and (iso) isolated system. Dashed lines give the range of uncertainty in the fraction of H II and composites caused by the double-nuclei galaxies with different spectral types for each nucleus. The single-merger stage combines the diffuse, compact, and old merger stages to ensure sufficient numbers of objects for statistically meaningful comparisons between the morphological types. There may be overlap between single-merger and isolated stages due to surface brightness effects.

(A color version of this figure is available in the online journal.)

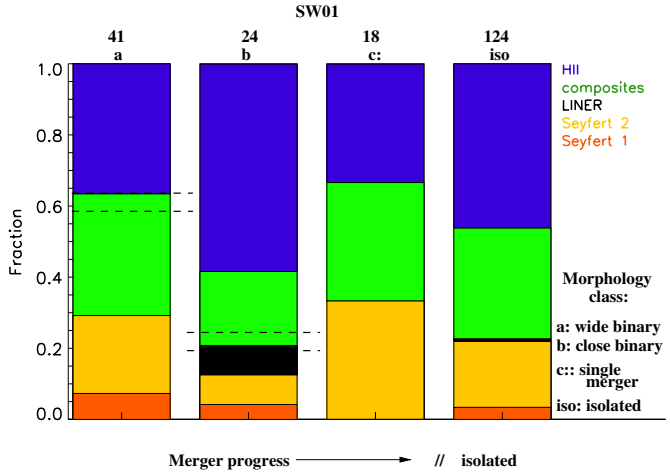


**Figure 10.** Optical spectroscopic classification as a function of merger morphology for the SW01 sample. The merger progresses from left to right: (a) wide binary, (b) close binary, (c) single merger, and (d) isolated. Dashed lines give the range of uncertainty in the fraction of H II and composites (in stage a), composite, and Seyferts (in stage b) caused by the double-nuclei galaxies with different spectral types for each nucleus. The single-merger stage combines the diffuse, compact, and old merger stages to ensure sufficient numbers of objects for statistically meaningful comparisons between the morphological types. The SW01 sample contains a substantial fraction (156/285 ∼ 54%) of apparently isolated galaxies. There may be overlap between single-merger and isolated stages due to surface brightness effects. The fraction of composites is not significant as compared to Figure 8.

(A color version of this figure is available in the online journal.)

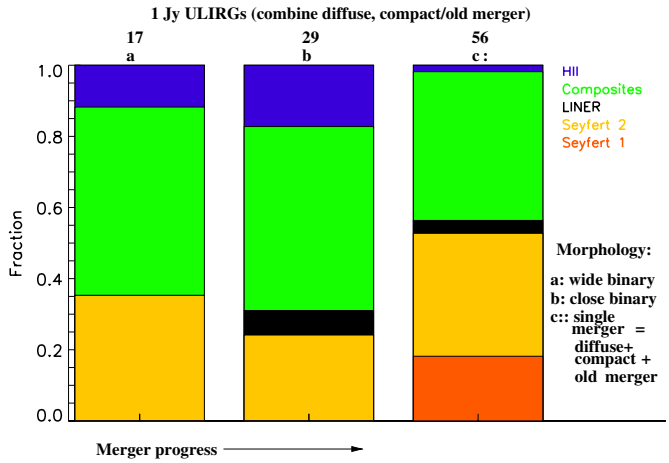


**Figure 11.** Optical spectroscopic classification as a function of merger morphology for the 1 Jy ULIRG sample, after combining the diffuse, compact, and old mergers as one single-merger category.

(A color version of this figure is available in the online journal.)

between the three late merger stages (diffuse, compact, and old merger) in non-ULIRG samples.

To conclude, the 1 Jy ULIRG sample shows a marked change in galaxy spectral type as a function of merger progress, especially, composite galaxies dominate the diffuse merger stage. It is unclear whether such a change occurs in the lower luminosity BGS and SW01 samples. We note that the relative lack of galaxies at late merger stages in the lower luminosity samples may indicate that a ULIRG phase occurs before or at the single-nucleus stage, in at least some IR-selected galaxies.

### 3.4. $D_{AGN}$ and $L_{IR}$ versus *ns*

To investigate the merger progress in a morphology-independent way, we compare the *relative* contribution of an AGN ($D_{AGN}$) and $L_{IR}$ as a function of projected nuclear separation (*ns*). We first investigate the non-ULIRG samples by combining the BGS and SW01 samples to (a) reach statistically significant conclusions (thus minimizing projection effects) and (b) span a broad range of $L_{IR}$. The *ns* values for both samples are measured using 2MASS or DSS images, and the two samples exhibit similar behavior in spectral type versus morphology as discussed in Section 3.3.

In Figure 12(a), we show the infrared luminosity, $L_{IR}$, of the merger pair as a function of nuclear separation. Figure 12(b) gives $D_{AGN}$ as a function of nuclear separation for the BGS (LIRGs) and the SW01 samples combined. These figures indicate that $D_{AGN}$ is constant at ∼0.3 within the errors at all merger stages in these two samples. The mean value of $L_{IR}$

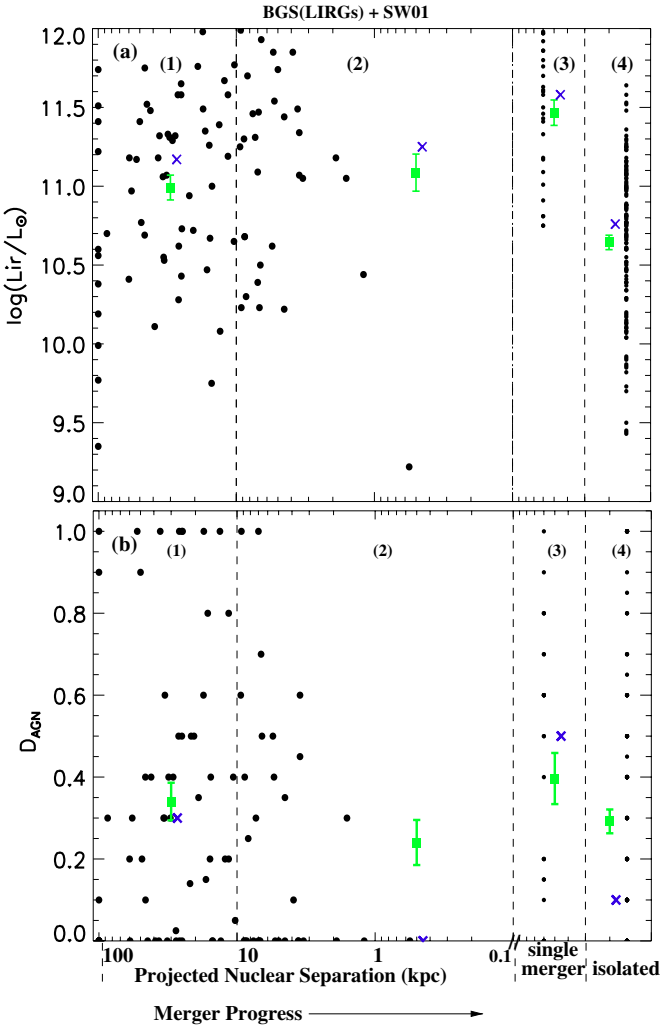


**Figure 12.** (a) $L_{IR}$ as a function of projected nuclear separation for the BGS (LIRGs only) and SW01 samples combined. (b) Distance from the starburst sequence $D_{AGN}$ as a function of projected nuclear separation for the combined BGS (LIRGs only) and SW01 samples. The mean and $1\sigma$ standard deviation of the mean for $D_{AGN}$ are plotted as green squares. Median values are shown as blue crosses. The vertical regions from left to right are: (1) binary systems with nuclear separation $ns > 10$ kpc, (2) binary systems with nuclear separation $ns < 10$ kpc, (3) single-merger systems, and (4) isolated systems. The BGS and SW01 samples are combined in order to get a larger non-ULIRG sample. For the 21 overlap objects in the two samples, mean values of $D_{AGN}$ are taken. K-S tests for the significance of the difference in $y$-axis distributions are given in Section 3.4.

(A color version of this figure is available in the online journal.)

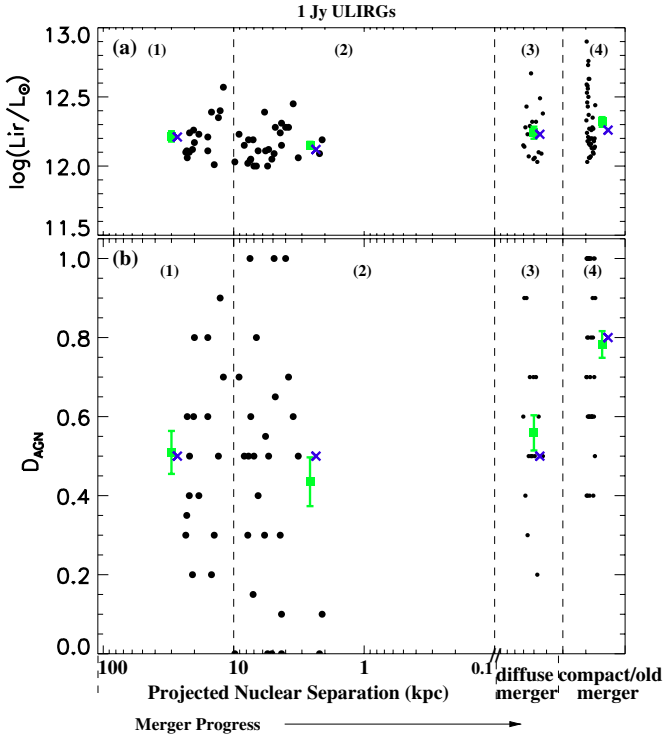


**Figure 13.** (a) $L_{IR}$ as a function of projected nuclear separation for the 1Jy ULIRGs. (b) Distance from the starburst sequence $D_{AGN}$ as a function of projected nuclear separation for the 1 Jy ULIRG sample. The means and $1\sigma$ standard deviation of the mean for $D_{AGN}$ are plotted as green squares. Median values are shown as blue crosses. The vertical regions from left to right are: (1) binary systems with nuclear separation $ns > 10$ kpc, (2) binary systems with nuclear separation $ns < 10$ kpc, (3) single mergers with diffuse nuclei, and (4) single mergers with compact/old nuclei. K-S tests for the significance of the difference in $y$-axis distributions are given in Section 3.4.

(A color version of this figure is available in the online journal.)

is constant within the errors through the wide and close pair stages, and then rises by a factor of ∼2 in the single-merger stage. We performed K-S tests to determine the significance of the distribution of $D_{AGN}$ and $L_{IR}$ as a function of projected separation. For the distribution of data within adjacent $L_{IR}$ bins (1) and (2), (2) and (3), and (3) and (4) in Figure 12(a), the K-S test indicates a probability $P_{null} = 0.89$, 0.04, and 3.8E−9, respectively, that the adjacent data sets are drawn from the same parent population. For the adjacent $D_{AGN}$ bins (1) and (2), (2) and (3), (3) and (4) in Figure 12(b), the K-S test indicates a probability $P_{null} = 0.13$, 0.18, and 0.16 that the adjacent data sets are drawn from the same parent population. We conclude that both the rise in $L_{IR}$ from close pair to single-merger stage and the fall in $L_{IR}$ from single merger to isolated stages are significant at the 95% and 99.99% level, respectively. There are no statistically significant changes in $D_{AGN}$ as a function of projected separation for the non-ULIRG BGS and SW01 samples.

In Figures 13(a) and (b), we show the $L_{IR}$ and $D_{AGN}$ versus projected separation for the 1 Jy ULIRG sample. Like the lower luminosity pairs, $D_{AGN}$ is constant within the errors as a function of projected separation until the diffuse merger stage. The mean $D_{AGN}$ is larger than seen in the lower luminosity BGS+SW01 sample (∼0.52 compared to 0.3). The most obvious difference in the behavior of ULIRGs with projected separation compared with the lower luminosity pairs, occurs in the final compact/old merger phase where ULIRGs show a rather dramatic increase in $D_{AGN}$ to a mean value of ∼0.8. This rise is statistically significant at the 95% level; the K-S test indicates a probability $P_{null} = 0.46$, 0.51, and 0.05 that adjacent data sets (1-2), (2-3), and (3-4) are drawn from the same parent population. This rise in $D_{AGN}$ is consistent with the rise in the Seyfert fraction with merger progress seen in Section 3.3, particularly in the emergence of Seyfert 1s at the compact and old merger stages. The rise in $D_{AGN}$ is not accompanied by a significant rise in the mean $L_{IR}$ (the K-S test indicates a probability $P_{null} = 0.52$, 0.12, and 0.84 that the adjacent data sets (1-2), (2-3), and (3-4) are drawn from the same parent population).

Our results confirm previous observational (e.g., Sanders et al. 1988a) and theoretical (e.g., Mihos & Hernquist 1994) studies showing that the maximum $L_{IR}$ is produced close to the time when the two nuclei merge.

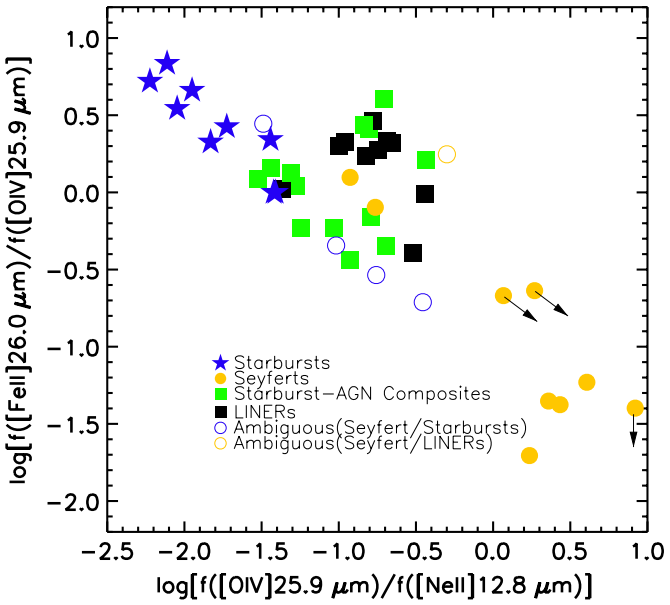


**Figure 14.** Mid-infrared diagnostic from Sturm et al. (2006), with objects reclassified using the Ke06 new scheme. The data were provided by E. Sturm. The symbol meanings are labeled on the plot. The bracket after the ambiguous class indicates between which classes the ambiguity lies.

(A color version of this figure is available in the online journal.)

## 4. DISCUSSION

### *4.1. IR-selected LINERs*

We find that IR-luminous LINERs are rare compared to other optical spectral types, even in the low-redshift BGS sample. A majority of the previously classified IR-luminous LINERs are now reclassified as starburst–AGN composites in the new SDSS optical spectroscopic classification scheme. This result prompts us to discuss the following issues: (1) the relationship between the new class of LINERs and starburst–AGN composite objects; (2) the nature of IR-luminous LINERs compared with the LINERs from the SDSS. We discuss each of these issues separately below.

1. Kewley et al. (2006) have shown that the host properties of composite galaxies are intermediate between those of AGN and high-metallicity star-forming galaxies, and that LINERs form a unique, coherent class that is distinct from Seyferts, star-forming galaxies and composites. Specifically, LINERs are older, more massive, less dusty, and less concentrated than Seyfert galaxies. These optical results highlight the intrinsically different nature of LINERs and composites.

   Here we investigate whether similar differences exist in popular mid-IR diagnostics. In Figure 14, we investigate the positions of galaxies on the [Fe III] 26.0 $\mu$m/[O IV] 25.9 $\mu$m versus [O IV] 25.9 $\mu$m/[Ne III] 12.8 $\mu$m diagnostic diagram. This diagram separates star-forming galaxies from those dominated by an AGN. Previously, IR-luminous LINERs occupied a region in between starburst and Seyfert galaxies, whereas IR-faint LINERs occupied a region offset from the starburst–Seyfert sequence (Sturm et al. 2006). In our new classification scheme, only one out of the 16 IR-luminous LINERs are classified as LINERs (the rest 15 objects are eight composites, one Seyfert 2s, and six ambiguous classes between H II and Seyfert 2s), while 10 out of the 17 IR-faint LINERs remain LINERs (the rest seven objects are ambiguous classes between LINERS and Seyfert 2s). Figure 14 indicates that the majority (9/13) of the composites lie along a mixing sequence connecting star-forming galaxies and Seyferts. By contrast, most (8/10) of the LINERs lie offset from the mixing sequence. These results are consistent with our view of optically selected LINERs as a different class of objects from starburst–AGN composites.
2. There is growing evidence that a large fraction of optically selected LINERs are low-luminosity AGNs with low accretion rates (e.g., Ho 1999; Quataert 2001; Barth 2002). The SDSS LINER population studied by Kewley et al. (2006) supports this AGN nature. They show that at fixed $L$[O III]/$\sigma^4$ (an indicator for the black hole accretion rate), all differences between Seyfert and LINER host properties disappear. With this interpretation of LINERs, it is not surprising that we find so few IR-luminous LINERs because ULIRGs tend to harbor AGN that favor high-accretion rates (Weedman 1983; Filippenko & Sargent 1985; Sanders et al. 1988a). Theory supports this interpretation; numerical simulations predict that the black hole accretion rate rises rapidly during the merger process when enormous quantities of gas flows into the central regions of the merging galaxies (e.g., Taniguchi et al. 1999; Hopkins et al. 2005).

What about the few IR-luminous LINERs that do exist in our samples? Do they belong to the same class as optical LINERs? In Table 9, we list all the possible LINERs found in our combined 1 Jy ULIRG + BGS + SW01 sample. Altogether there are nine objects in the three samples that fall into our LINER class, however, only 4/9 of these LINERs (Arp 220 in the 1 Jy ULIRG sample, NGC 6240 in the SW01/BGS samples, and another three in the BGS sample) can be "safely" classified as LINERs. The other 5/9 LINERs lie near the 0.1 dex error region of the Seyfert–LINER boundaries, and may be Seyfert objects or intermediate between Seyfert and LINER types. This can be clearly seen in Figure 15, where all nine LINERs are over-plotted with the SDSS data from Kewley et al. (2006) on the [S II]/H$\alpha$ versus [O III]/H$\beta$ and [O I]/H$\alpha$ versus [O III]/H$\beta$ diagnostic diagrams.

In Figure 15, we indicate the positions of two well-studied IR-luminous LINERs: NGC 6240 and Arp 220. Recent high-resolution X-ray and radio data for NGC 6240 (Lira et al. 2002; Komossa et al. 2003; Iono et al. 2007) and Arp 220 (Clements et al. 2002; Ptak et al. 2003; Downes & Eckart 2007) provide convincing evidence for the existence of AGN in these two objects. However, the LINER emission may be excited by other ionization processes. Both of these two LINERs show evidence for starburst-driven superwinds and/or shocks that may dominate the EUV emission of these galaxies (Heckman et al. 1987; Tecza et al. 2000; Lira et al. 2002; McDowell et al. 2003; Iwasawa et al. 2005). Further investigation into the EUV power source of IR-luminous LINERs is required to draw robust conclusions about the nature of the few IR-luminous LINERs in our samples.

To summarize, the rarity of IR-luminous LINERs is consistent with the picture that most LINERs are (a) excited by low Eddington rate black holes and (b) reside in galaxies with an aged stellar population. The special cases of Arp 220 and NGC 6240 may indicate a contribution from different LINER ionization sources: either starburst superwinds or shocks driven by galaxy collisions.

**Table 9**
Properties of LINERs in the three Samples

| Name | $d_{[O\,I]}$[a](dex) | $d_{[S\,II]}$(dex) | log ($L_{IR}/L_{\odot}$) | Morphology |
|---|---|---|---|---|
| | | 1 Jy ULIRGs | | |
| IRAS 14504−1958 | 0.05 | 0.02 | 12.12 | ... |
| IRAS 04074−2801 | 0.15 | 0.18 | 12.14 | Diffuse merger |
| IRAS 15327+2340 (Arp220) | 0.31 | 0.34 | 12.17 | Close binary, $ns = 0.0$ kpc |
| | | SW01 | | |
| IRAS 05497−0728 (NGC2110) | 0.07 | 0.08 | 10.08 | ... |
| IRAS 16504+0228 (NGC6240) | 0.4 | 0.28 | 10.86 | Close binary, $ns = 0.74$ kpc |
| IRAS 16399−0937, object2 | 0.05 | 0.08 | 11.07 | ... |
| | | BGS | | |
| IRAS 05187−1017 | 0.17 | 0.12 | 11.23 | Isolated? |
| IRAS 01364−1042 | 0.35 | 0.05 | 11.76 | ... |
| IRAS 03134−0236 (NGC1266) | 0.13 | 0.44 | 10.34 | Isolated? |
| IRAS 22359−2606 (ESO534-G009) | 0.54 | 0.32 | 10.61 | Isolated? |

**Notes.** General properties of the nine LINERs classified by the new scheme in the three samples.
[a] Index distance from the Seyfert–LINER classification line in the BPT [O I] diagram. Available morphology information comes from images in NED.

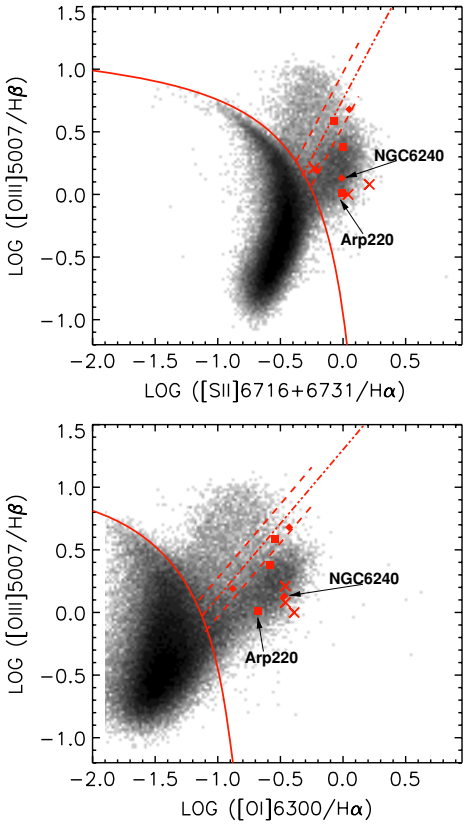


**Figure 15.** Positions of the nine LINERs on the [S II]/H$\alpha$ vs. [O III]/H$\beta$ and [O I]/H$\alpha$ vs. [O III]/H$\beta$ diagrams over-plotted on the SDSS data from Kewley et al. (2006). The three IR-luminous LINERs in the 1 Jy ULIRG sample are shown as squares, the three IR-luminous LINERs in the SW01 sample are shown as diamonds, and the three crosses are the IR-luminous LINERs from the BGS sample.

(A color version of this figure is available in the online journal.)

### *4.2. Are Starburst–AGN Composites Playing the Role of "Bridging" in LIRGs and ULIRGs?*

In Figure 16, we show five different galaxy samples on the [N II]/H$\alpha$ versus [O III]/H$\beta$ diagnostic diagram. The new Ke06 classification boundaries are indicated in red. We supplement the 1 Jy ULIRG, BGS and SW01 samples with two optically selected samples: the NFGS field galaxy sample (Jansen et al. 2000) and the BGK00 galaxy close pair sample (Barton et al. 2000). The samples in Figure 16 are ordered from (a) to (e) by the level of interaction activity—from no interaction (NFGS field galaxies), to non-IR-selected galaxy pairs, to luminous IR-selected galaxies, and to the most luminous IR-selected galaxies (1 Jy ULIRGs).

The fraction of starburst–AGN composite galaxies increases from the field galaxy sample (3.6%) → galaxy pair sample (22.8%) → SW01 galaxies (29.6%) → BGS galaxies (dominated by LIRGs) (37%) → 1 Jy ULIRGs (49.1%). This plot indicates that the stronger the interaction between galaxies is, the more likely they are to contain starburst–AGN composite galaxies.

Our new results offer some hope for resolving previous disputes concerning the evolution of starburst and AGN activity in gas-rich major mergers, in particular for ULIRGs. We have shown that a large fraction of ULIRGs are of composite starburst–AGN spectral type, with line ratios (or $D_{AGN}$) indicating an intermediate class between pure starbursts and pure AGN. Spectral classification as a function of merger evolution does not change abruptly from "pure" starburst into "pure" AGN. ULIRGs may spend a fairly large fraction of their merger history in a phase where starburst and AGN both make significant contributions to the EUV radiation. In luminous IR mergers, starburst–AGN composites appear to "bridge" the spectral evolution from pure starburst to AGN-dominated activity as the merger progresses. For ULIRGs, we have shown that an initial apparent decrease in starburst activity from the wide binary to close binary stage is accompanied by a rise in the starburst–AGN composites. Similarly, as the merger reaches its final stages, the fall in starburst–AGN composites is followed by a rise in Seyfert activity. These effects can be seen in Figure 8, where the starburst–AGN composite activity peaks in the diffuse merger stage. We do not have sufficient data to determine whether a similar scenario occurs at the lower IR luminosities spanned by the BGS and SW01 samples ($L_{IR} < 10^{12}\ L_{\odot}$).

### *4.3. The Merger Scenario for LIRGs → ULIRGs*

There is now substantial agreement that ULIRGs are triggered by major mergers of gas-rich spirals (see the review by Sanders

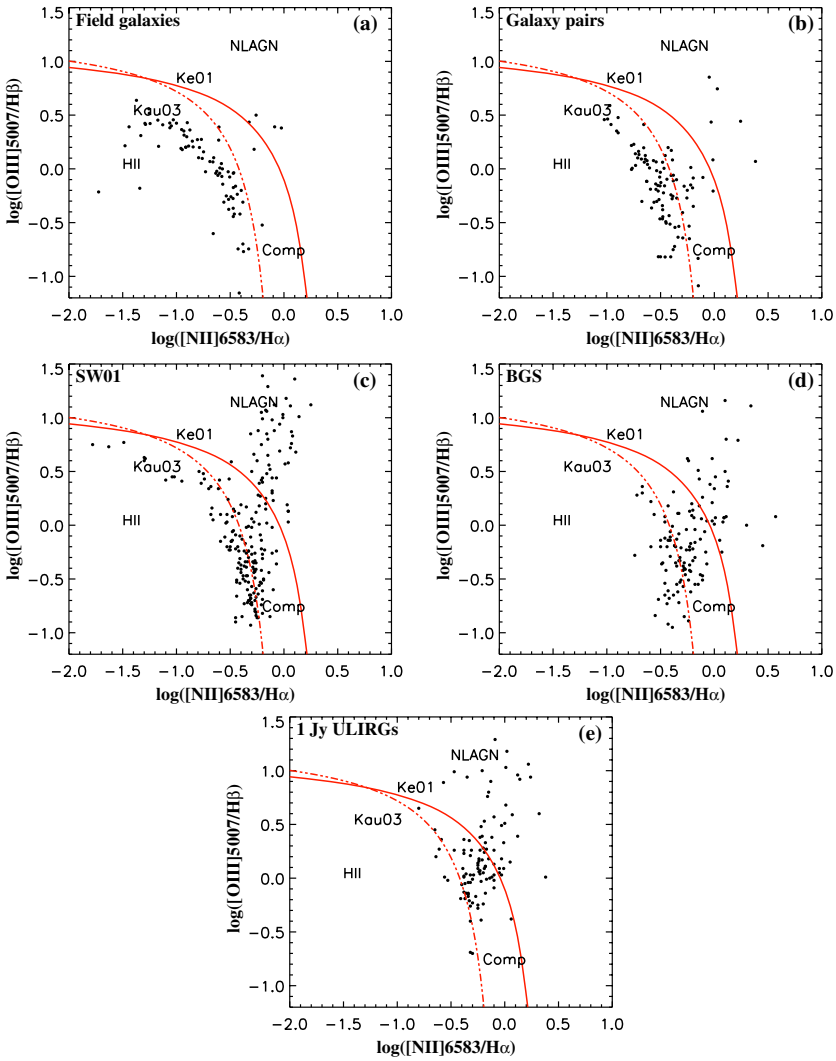


**Figure 16.** Composite galaxies on the "[N II] diagram" for different types of galaxy samples. (a) Field galaxy sample: NFGS (Jansen et al. 2000), (b) galaxy pair sample: BGK00 (Barton et al. 2000), (c) SW01 sample, (d) BGS sample, and (e) 1 Jy ULIRG sample.

(A color version of this figure is available in the online journal.)

& Mirabel 1996). In this merger scenario, the LIRG phase begins when tidal interactions between merging gas-rich disk galaxies initially trigger widespread starburst activity in one or both disks. As the merger progresses, gas is funneled toward the merger nucleus and activates nuclear starbursts and AGN, further increasing the IR luminosity. However, many questions still remain. The precise link between AGN fueling, the gas dynamics, and star formation either on a nuclear or a global scale is still poorly determined. The relative strength of starburst and AGN activity, particularly in the ULIRGs is still debated, and the question of whether the majority of LIRG mergers become ULIRGs has not been clearly addressed.

Our new results shown in Figures 9–16 provide new insight into how starburst and AGN activity evolve during interaction/merger of IR-luminous galaxies.

For lower luminosity IR galaxies ($L_{\rm IR} < 10^{12}\ L_{\odot}$), Seyferts are rare ($D_{\rm AGN} = 0.25$–$0.35$), and starbursts strongly contribute to the EUV radiation field either as "pure" starbursts or as composites. The majority of lower luminosity LIRGs are wide or close pairs. These pairs may either evolve into the single-merger stage without becoming ULIRGs, or they may enter the ULIRG phase during or shortly after the close pair stage. We consider both cases

1. Some lower luminosity IR galaxies ($L_{\rm IR} < 10^{12}\ L_{\odot}$) may reach the final single-merger stage without becoming ULIRGs. As these non-ULIRG galaxies evolve from the close pair to the single-merger stage, the mean IR luminosity increases by ∼2× (to $L_{\rm IR} \sim 10^{1}1.5\ L_{\odot}$), with only a relatively small rise in the mean value of $D_{\rm AGN}$(∼0.4). These results suggest that non-ULIRGs undergo a rise in starburst activity but only modest AGN growth as they evolve from the close pair to the single-merger stage. Some of these lower luminosity single mergers may be the product of minor mergers of objects with mass ratios larger than 5:1 (Ishida 2004; Ishida et al. 2009).
2. The lower luminosity pairs that may become ULIRGs are likely to be major mergers with mass ratios closer to unity (Ishida 2004; Ishida et al. 2009). In the ULIRG phase, the AGN contribution is elevated at all merger stages. We observe clear changes in the optical classification of ULIRGs as a function of merger stage. The diffuse merger stage (compared to the close binary stage) shows a dramatic increase in starburst–AGN composites (from ∼45% to ∼80%). In the subsequent compact/old merger stages, the fraction of composite galaxies falls, and AGNs dominate.

The mean value of $D_{AGN}$ rises (by ∼0.22 dex—from 0.43 to 0.65), and the mean value of $L_{IR}$ rises (∼1.7×), along with the emergence of a substantial Seyfert 1 fraction (∼25%). These results suggest that during the diffuse merger stage, the AGN becomes more powerful and increasingly visible via the optical emission-line ratios. Once the merged nucleus begins forming a core (compact merger stage), starburst activity may be subsiding (and possible dust obscuration clears) as AGN activity becomes prominent. We tentatively suggest that the dramatic increase in $D_{AGN}$ and the emergence of a substantial population of Seyfert 1s (accompanied by a ∼2× increase in $L_{IR}$) may signify a significant "blowout" phase, as ULIRGs transition to optical QSOs (e.g., Hopkins et al. 2005). A larger sample of ULIRGs is required to test this idea.

## 5. SUMMARY

We apply the new SDSS semi-empirical optical spectral classification scheme to three IR-selected galaxy samples—the 1 Jy ULIRG sample, the *IRAS* Bright Galaxy Sample, and the Southern Warm IR Galaxy Sample. Because the new classification scheme is substantially different from previous methods, the new scheme is used to yield insights into the relationship between starburst and AGN activity and merger progress. We utilize optical and near-IR images to determine the projected separation between pairs in our samples, and to classify the galaxies morphologically. The projected separation and morphological classification are used as relative tracers of merger progress. For each sample, we investigate how the optical classification and the relative AGN contribution, $D_{AGN}$, changes as a function of $L_{IR}$ and merger progress.

We find that

1. IR-luminous LINERs are rare; there are very few LINERs in the 1 Jy ULIRG, and the BGS and SW01 samples. The rarity of LINERs in the 1 Jy ULIRG and SW01 samples may be at least partly due to selection effects. Nearly all of the previously classified IR-luminous LINERs are starburst/AGN composite galaxies in the Ke06 classification scheme.
2. The new classification scheme reveals a clear evolutionary scenario for ULIRGs from starburst-driven activity in the early merger stages, composite starburst–AGN activity intermediate merger stages to AGN-dominated emission at late merger stages. The fraction of composite galaxies rises from 45% to 80% between the wide binary and diffuse merger stages and appears to "bridge" pure starburst and Seyfert galaxies. Galaxies at the diffuse merger stage are key for future investigations into the relationship between starburst and AGN activity in ULIRGs.
3. We find that advanced mergers preferentially occur in ULIRG samples. We suggest that the transition into the ULIRG phase occurs close to or during the diffuse merger stage in which the nuclei of the two merging galaxies are coalescing.
4. At later merger stages in ULIRGs, when the single nucleus is forming a core, the fraction of pure-Seyfert objects rises dramatically. This stage corresponds to the highest $L_{IR}$ in the 1 Jy ULIRG sample. At this stage, we propose that (a) starburst activity subsides, allowing the AGN to dominate the energy budget, and/or (b) dust obscuration surrounding the AGN clears, allowing the AGN radiation field to ionize the surrounding gas, and/or (c) AGN activity increases.
5. Seyfert 1s appear to occur only in the final "compact/old merging" stages of ULIRGs. A larger sample of Seyfert 1s is required to determine the significance of this result. If this result holds for larger samples, we hypothesize that a rise in Seyfert 1 galaxies at late merger stages may signify a significant "blowout" phase, as ULIRGs transition to optical QSOs.
6. There is no significant change in spectral types for the non-ULIRG BGS and SW01 samples.

Understanding the behavior of composite galaxies may help to build a more concrete picture of the merger process for all IR-luminous galaxies. Our future work includes integral field spectroscopy of composite galaxies and a detailed comparison between our results and the evolutionary merger models from numerical simulations (Barnes 2004; Hopkins et al. 2005, 2006a, 2006b, 2007, 2008).

We thank D.-C. Kim for providing the images for the 1 Jy ULIRG sample and E. Sturm for his mid-infrared data. We also thank T. Heckman for helpful comments. We are grateful to the referee for some very good suggestions/comments that significantly improved this paper. This work has made use of the DSSs that were produced at the Space Telescope Science Institute, under US government grant NAG W-2166, and the NASA/IPAC Extragalactic Database (NED), which is operated by the Jet Propulsion Laboratory, California Institute of Technology. The 2MASS data were obtained from the NASA/IPAC Infrared Science Archive, which is operated by the Jet Propulsion Laboratory, California Institute of Technology, under contract with NASA.

## APPENDIX A

## $D_{AGN}$ FROM DIFFERENT BPT DIAGRAMS

Theoretical models have shown that the distribution of galaxies on the BPT diagrams are mainly driven by variations of parameters such as metallicity, stellar age, ISM pressure, and ionization parameter (Dopita et al. 2000, 2006; Kewley 2001; Groves et al. 2004). The different sensitivity to these parameters of the four line ratios makes the three BPT diagrams distinct in distinguishing certain branches of galaxies.

Kewley et al. (2006) defined $D_{AGN}$ on the [O I]/H$\alpha$ diagram because the Seyfert and LINER branches are most clearly separated on the [O I]/H$\alpha$ diagram. In this case, $D_{AGN}$ can be defined separately for Seyferts and LINERs. The disadvantage of this diagram is that pure star-forming galaxies have to be removed first using the other two diagrams, because star-forming galaxies and starburst–AGN composites occupy similar regions on the [O I]/H$\alpha$ diagram.

The advantage of the [N II]/H$\alpha$ diagram is that the star-forming sequence is most tightly formed, giving a better contrast with the starburst–AGN branch. Also, [N II] has higher S/N than [O I]. However, in this diagram, Seyferts and LINERs cannot be well separated. We define $D_{AGN}$ on the [N II]/H$\alpha$ diagram in Figure 17: first, we empirically fit the SDSS star-forming sequence with a curve. Then, three points are chosen from the curve as "base points" (empty red circles in the lower left region in Figure 17). Another three "peak points" (empty red circles in the upper right region in Figure 17) are chosen from the upper right region of the diagram as $D_{AGN} = 1$. These points construct three "evolutionary line" intervals (lines a, b, and c in Figure 17). We divide the intervals equally into 10 bins which define regions for different values of $D_{AGN}$, e.g., for the region

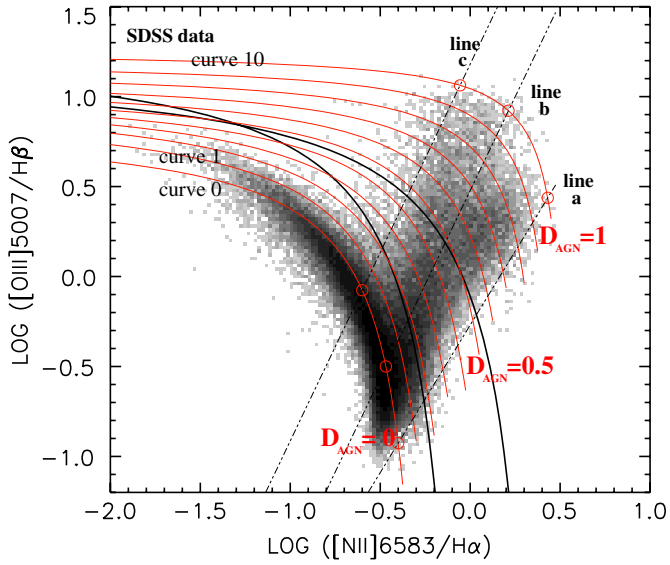


**Figure 17.** $D_{\rm AGN}$ defined on the "[N II]" diagram. "Base" and "peak" points are chosen to fit the outer boundary of the star-forming sequence and the $D_{\rm AGN} = 1$ curve. The regions between the boundary and curve are then divided into 10 bins to define the value of $D_{\rm AGN}$.

(A color version of this figure is available in the online journal.)

below curve 0, $D_{\rm AGN} = 0$; for the region above curve 0 and below curve 1, $D_{\rm AGN} = 0.1$,..., and $D_{\rm AGN} = 1$ for the region above curve 10. Note that $D_{\rm AGN}$ is defined differently from the "radial-arc" system used in Kewley et al. (2006), specifically for the [O I]/H$\alpha$ diagram, because the starburst–AGN branch does not simply develop from one base point on the [N II]/H$\alpha$ diagram.

We list the $D_{\rm AGN}$ defined on both diagrams in Tables 1–3. There is little difference in the two differently defined $D_{\rm AGN}$, however, it is not meaningful to compare the absolute value of $D_{\rm AGN}$. As emphasized in the text, only the relative value of $D_{\rm AGN}$ is useful. As an example, we show in Figure 18 that our results in Section 3.4 do not change when we apply the $D_{\rm AGN}$ defined on the [N II]/H$\alpha$ diagram. Defining $D_{\rm AGN}$ on the [S II]/H$\alpha$ diagram does not change the results.

There is a good relation between $D_{\rm AGN}$ and spectral types: the mean value of $D_{\rm AGN}$ increases from star-forming galaxies, to starburst–AGN composites, and to Seyfert 2 and LINERs. Table 10 lists the spectral types and their corresponding mean

**Table 10**
Spectral Type and $D_{\rm AGN}$

| Spectral Type | $D_{\rm AGN}$ | |
|---|---|---|
| | Mean | Median |
| Starburst (H II region) | 0.2(0.2) | 0(0.2) |
| Starburst–AGN composite | 0.4(0.4) | 0.3(0.4) |
| LINER | 0.8(0.8) | 0.9(0.9) |
| Seyfert 2 | 0.8(0.7) | 0.8(0.7) |

**Notes.** Column 1: spectral types defined using the Ke06 semi-empirical scheme; Column 2: $D_{\rm AGN}$ median value; Column 3: $D_{\rm AGN}$ mean value. Based on 420 galaxies from the 1 Jy ULIRG, BGS, and SW01 samples. Seyfert 1 objects are set to have $D_{\rm AGN} \equiv 1$.

and median $D_{\rm AGN}$. The values are based on ∼400 galaxies from the 1 Jy ULIRG, BGS, and SW01 samples, as given in Tables 1, 2, and 3. Star-forming galaxies have $D_{\rm AGN} \leqslant 0.2$, starburst–AGN composites have a mean $D_{\rm AGN} = 0.4(0.4)$, and Seyferts/LINERs have $D_{\rm AGN} = 0.7(0.8)$. We assign $D_{\rm AGN} = 1$ to Seyfert 1 objects since they are not included in the BPT diagrams and are almost certainly dominated by an AGN.

## APPENDIX B

## CLASSIFICATION CRITERIA AND "AMBIGUOUS" CLASS

In Section 2.2, we use the 2-of-3 criterion to assign a class to our samples, based on agreement between two out of the three standard optical diagnostic diagrams. The 2-of-3 criterion has two advantages: (1) the final classification is less sensitive to low S/N in either [O I] or [S II] which may sometimes be weak, and (2) galaxies without [S II] or [O I] measurements can be assigned a class based on the remaining one or two diagnostic diagrams.

In Figure 19, we show the galaxies in the three samples classified using the 2-of-3 criterion on the BPT diagrams. As outlined in Kewley et al. (2006), the [N II]/H$\alpha$ line ratio is more sensitive to the presence of low-level AGN than [S II]/H$\alpha$ or [O I]/H$\alpha$ because [N II]/H$\alpha$ is more sensitive to metallicity. The log([N II]/H$\alpha$) line ratio is a linear function of the nebular metallicity until high metallicities where the log([N II]/H$\alpha$) ratio saturates. This saturation point causes the star-forming sequence to be almost vertical at log([N II]/H$\alpha$) = −0.5. Any AGN contribution moves [N II]/H$\alpha$ above this saturation level,

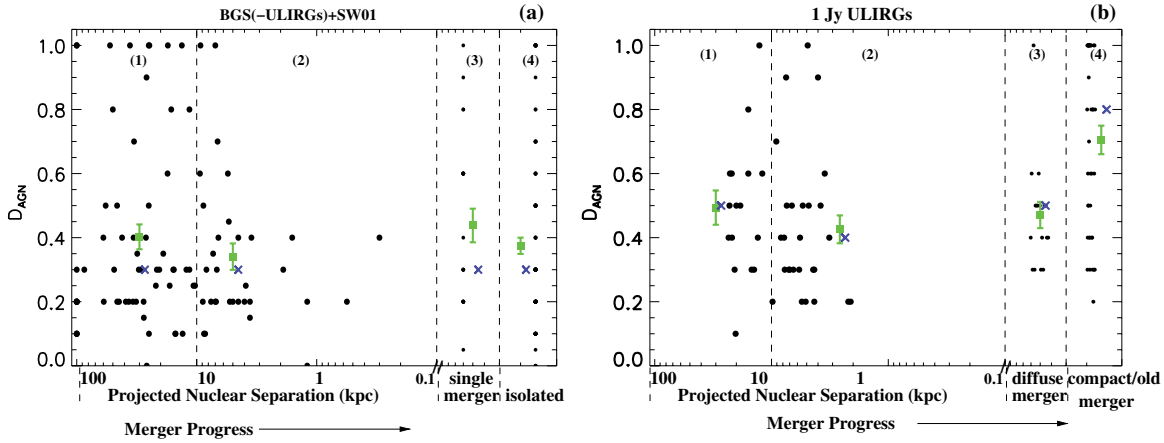


**Figure 18.** As in Figures 12 and 13, but using $D_{\rm AGN}$ as defined on the [N II]/H$\alpha$ diagram.

(A color version of this figure is available in the online journal.)

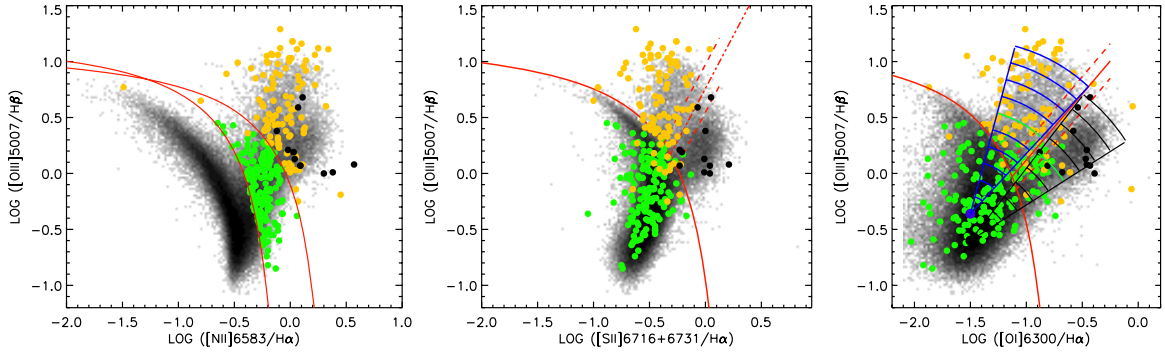


**Figure 19.** Classified galaxies in the three samples using the 2-of-3 criterion. Green: composites. Orange: Seyfert 2. Black: LINERs. Solid red lines are the new classification boundaries as in Figure 1. Wedges on the [O I]/H$\alpha$ diagram are used to derive $D_{\rm AGN}$ as described in Figure 3.
(A color version of this figure is available in the online journal.)

allowing the identification of galaxies with even small AGN contributions.

The [S II]/H$\alpha$ and [O I]/H$\alpha$ line ratios cannot be used to distinguish composite galaxies from pure star-forming galaxies. In the [S II]/H$\alpha$ and [O I]/H$\alpha$ diagnostic diagrams, composite galaxies occupy a region that is degenerate with the star-forming galaxy sequence. This problem is caused by the relationship between [S II]/H$\alpha$ and [O I]/H$\alpha$ and metallicity. The AGN–starburst mixing sequence begins at the high-metallicity end of the star-forming galaxy sequence. The [S II]/H$\alpha$ and [O I]/H$\alpha$ line ratios (unlike the [N II]/H$\alpha$ ratio) are double valued with metallicity over the range of observed [S II]/H$\alpha$ and [O I]/H$\alpha$ ratios in nearby galaxies. The highest metallicity star-forming galaxies occur at low [S II]/H$\alpha$ and [O I]/H$\alpha$ ratios (log([S II]/H$\alpha$) = $-0.6$ to $-0.9$, and log([O I]/H$\alpha$) = $-2.0$ to $-1.4$) (see Figures in Dopita et al. 2000; Kewley 2001). Therefore, a large AGN contribution (~40%–50%) is required for a composite galaxy to rise above the star-forming galaxy sequence.

The 3-of-3 criterion is a more stringent method of classification that is based on all three diagnostic diagrams. This method allows ambiguous galaxies to be classified as those galaxies that have one classification in one or two diagrams and a different classification in the remaining diagram(s). The 3-of-3 criterion is suitable for galaxies with high S/N spectra where all five diagnostic emission lines have S/N > 3 (e.g., Kewley et al. 2006). Samples with lower S/N emission lines may contain a large fraction of ambiguous galaxies if the 3-of-3 criterion is applied.

According to the 3-of-3 scheme, the 1 Jy ULIRGs contain four (4.0%) H II-region galaxies, 18 (18%) starburst–AGN composites, 23 (23%) Seyfert 2, 10 (10%) Seyfert 1, and three (3%) LINERs. The remaining 41 (41%) galaxies are ambiguous, illustrating the effect of low S/N for the [S II] and/or [O I] emission lines in this sample.

For the LIRGs in the BGS sample, a total of 74 single-nucleus galaxies have measured spectra on all three diagrams. Using the 3-of-3 criterion, 22 (29.7%) are H II-region galaxies, 19 (25.7%) are starburst–AGN composites, eight (10.8%) are Seyfert 2, one galaxy (1.4%) is a Seyfert 1, and five (6.7%) are LINERs. The remaining 19 (25.7%) galaxies are ambiguous.

For the SW01 sample, a total of 175 single-nucleus objects that have measured emission-line fluxes with S/N > 3$\sigma$. The majority of the sample has S/N > 8$\sigma$ for all five diagnostic lines. In the 3-of-3 scheme, we obtain 70 (40.0%) H II-region galaxies, 48 (27.4%) starburst–AGN composites, 33 (18.9%) Seyfert 2, 10 (5.7%) Seyfert 1, and two (1.1%) LINERs. The remaining 12 (6.8%) galaxies are ambiguous.

With the 3-of-3 criterion, we obtain a large fraction of ambiguous galaxies in the ULIRGs and BGS samples (41% and 25.7%, respectively), while the fraction of ambiguous galaxies in the SW01 sample is relatively small (7%). The fraction of ambiguous galaxies in the SW01 sample is consistent with the fraction of ambiguous galaxies in the SDSS where an S/N > 3 cut has been applied.

Among the ambiguous galaxies in the ULIRGs, 68% are ambiguous between composites and Seyferts/LINERs, i.e., they lie within the composite galaxy region on the [N II]/H$\alpha$ diagram, but lie above the Ke01 line on either (or both) the [S II]/H$\alpha$ or the [O I]/H$\alpha$ diagram. Many of these galaxies lie within the $\pm$0.1 dex error region of either (or both) the [S II]/H$\alpha$ or the [O I]/H$\alpha$ classification line and hence their classification with these diagram(s) is uncertain. Hill et al. (1999, 2001) investigate ambiguous galaxies using near-infrared spectroscopy and radio observations. They conclude that ambiguous galaxies are starburst–AGN composites. *Spitzer* spectroscopy of our ambiguous 1 Jy ULIRGs supports this conclusion; 5/6 of the ULIRG ambiguous galaxies observed by Imanishi et al. (2007) have evidence (either strong or tentative) of a buried AGN. Our results are unchanged if the 3-of-3 criterion is applied and if the ambiguous galaxies found using this criterion are starburst–AGN composites.

## APPENDIX C

## DOUBLE-NUCLEI GALAXIES WITH DIFFERENT SPECTRAL TYPES

There are 23 double-nuclei galaxies in the BGS. Of these, 13 have the same spectral type for the two nuclei (seven H II, six composites). For the remaining 10 galaxies, five have classes available only for one nucleus (four H II, one composite); the remaining five have different spectral types for each nucleus (one composite/H II, two composite/Seyfert 2, and two H II/Seyfert 2). There are nine double-nuclei galaxies in the 1 Jy sample. A total of four of these double-nuclei galaxies have the same spectral type for each nucleus (composite). The remaining 5/9 1 Jy ULIRGs all have a composite class for one nucleus (three composite/H II, two composite/Seyfert 2). There are 17 double-nuclei galaxies in the SW01 sample. A total of 13 of these double-nuclei galaxies have the same spectral type (eight H II, three composite, two Seyfert 2). Only four of the 17 double-nuclei galaxies in SW01 have different spectral types (one composite/LINER, two composite/H II, and one H II/Seyfert 2).

There are only 14 objects across all three samples that have different spectral types for each nucleus. We estimate the ranges

of uncertainty in our composite classification by first assigning all the double-nuclei galaxies with different spectral types as composites in order to derive an upper limit for the "composite" fraction. We next assign all of the double-nuclei galaxies with different spectral types the alternative types listed above to derive a lower limit of the "composite" fraction. The change in the fraction (shown as dashed lines in Figures 8–11) of the composite galaxies indicates the range of uncertainty introduced by these 14 objects.

## REFERENCES


Armus, L., Heckman, T. M., & Miley, G. K. 1990, ApJ, 364, 471
Baldwin, J., Phillips, M., & Terlevich, R. 1981, PASP, 93, 5 (BPT)
Barnes, J. E. 2004, MNRAS, 350, 798
Barnes, J. E., & Hernquist, L. E. 1992, ARA&A, 30, 705
Barnes, J. E., & Hernquist, L. E. 1996, ApJ, 471, 115
Barth, A. J. 2002, in ASP Conf. Ser. 258, Issues in Unification of Active Galactic Nuclei, ed. R. Maiolino, A. Marconi, & N. Nagar (San Francisco, CA: ASP), 147
Barton, E. J., Geller, M. J., & Kenyon, S. J. 2000, ApJ, 530, 660
Becklin, E. E., Frogel, J. A., Kleinmann, D. E., Neugebauer, G., Ney, E. P., & Strecker, D. W. 1971, ApJ, 170, L15
Becklin, E. E., & Neugebauer, G. 1972, BAAS, 4, 224
Bonatto, C. J., & Pastoriza, M. G. 1997, ApJ, 486, 132
Borne, K. D., Bushouse, H., Lucas, R. A., & Colina, L. 2000, ApJ, 529, L77
Bushouse, H. A. 1987, ApJ, 320, 49
Clements, D. L., & Baker, A. C. 1996, A&A, 314, 5
Clements, D. L., McDowell, J. C., Shaked, S., Baker, A. C., Borne, K., Colina, L., Lamb, S. A., & Mundell, C. 2002, ApJ, 581, 974
Clements, D. L., Sutherland, W. J., McMahon, R. G., & Saunders, W. 1996, MNRAS, 279, 477
Dasyra, K. M., et al. 2006, ApJ, 638, 745
Denicoló, G., Terlevich, R., & Terlevich, E. 2002, MNRAS, 330, 69
Dopita, M. A., Kewley, L. J., Heisler, C. A., & Sutherland, R. S. 2000, ApJ, 542, 224
Dopita, M. A., et al. 2006, ApJS, 167, 177
Downes, D., & Eckart, A. 2007, A&A, 468, 57
Farrah, D., Afonso, J., Efstathiou, A., Rowan-Robinson, M., Fox, M., & Clements, D. 2003, MNRAS, 343, 585
Farrah, D., et al. 2001, MNRAS, 326, 1333
Farrah, D., et al. 2007, ApJ, 667, 149
Filippenko, A., & Sargent, W. L. 1985, ApJS, 57, 503
Garcia, A. M. 1993, A&AS, 100, 47
Genzel, R., et al. 1998, ApJ, 498, 579
Giuricin, M., Mardirossian, F., & Mezzetti, M. 1995, ApJ, 446, 550
Goldader, J. D., Joseph, R. D., Doyon, R., & Sanders, D. B. 1995, ApJ, 444, 97
Goto, T. 2005, MNRAS, 360, 322
Groves, B. A., Dopita, M. A., & Sutherland, R. S. 2004, ApJS, 153, 9
Groves, B. A., Heckman, T. M., & Kauffmann, G. 2006, MNRAS, 371, 1559
Haas, M., Seibenmorgen, R., Pantin, E., Horst, H., Smette, A., Kaufl, H.-U., Lagage, P.-O., & Chini, R. 2007, A&A, 473, 369
Heckman, T. 1995, ApJ, 446, 101
Heckman, T., Timothy, M., Armus, L., & Miley, G. K. 1987, AJ, 93, 276
Heisler, C. A., & Vader, J. P. 1995, A&A, 110, 87
Hill, T. L., Heisler, C. A., Norris, R. P., Reynolds, J. E., & Hunstead, R. W. 2001, AJ, 121, 128
Hill, T. L., Heisler, C. A., Sutherland, R. P., & Hunstead, R. W. 1999, AJ, 121, 128
Ho, L. C. 1999, Adv. Space Res., 23, 813
Hopkins, P. F., Bundy, K., Hernquist, L., & Ellis, R. S. 2007, ApJ, 659, 976
Hopkins, P. F., Hernquist, L., Cox, T. J., & Keres, D. 2008, ApJS, 175, 356
Hopkins, P. F., Hernquist, L., Cox, T. J., Matieo, T. D., Martini, P., Robertson, B., & Springel, V. 2005, ApJ, 630, 705
Hopkins, P. F., Hernquist, L., Cox, T. J., Matieo, T. D., Robertson, B., & Springel, V. 2006a, ApJS, 163, 1
Hopkins, P. F., Somerville, R. S., Hernquist, L., Cox, T. J., Robertson, B., & Li, Y. 2006b, ApJ, 625, 864
Imanishi, M., Dudley, C. C., Maiolino, R., Maloney, P. R., Nakagawa, T., & Risaliti, G. 2007, ApJS, 171, 72
Iono, D., et al. 2007, ApJ, 659, 283
Ishida, C. M. 2004, PhD thesis, Univ. of Hawaii
Ishida, C. M., et al. 2009, ApJS, submitted
Iwasawa, K., Sanders, D. B., Evans, A. S., Trentham, N., Miniutti, G., & Spoon, H. W. W. 2005, MNRAS, 357, 565
Jansen, R. A., Franx, M., Fabricant, D., & Caldwell, N. 2000, ApJS, 126, 271
Joseph, R. D. 1999, A&SS, 266, 321
Kauffmann, G., et al. 2003, MNRAS, 346, 1055
Kawakatu, N., Anabuki, N., Nagao, T., Umemura, M., & Nakagawa, T. 2006, ApJ, 637, 104
Keel, W. C. 1983, ApJ, 269, 466
Kennicutt, R. C., & Keel, W. C. 1984, ApJ, 279, 5
Kennicutt, R. C., et al. 1987, AJ, 93, 1011
Kewley, L. J. 2001, PhD thesis, Australian National University
Kewley, L. J., & Dopita, M. A. 2002, ApJS, 142, 35
Kewley, L. J., Dopita, M. A., Sutherland, R. S., Heisler, C. A., & Trevena, J. 2001a, ApJ, 556, 121
Kewley, L. J., Groves, B., Kauffmann, G., & Heckman, T. 2006, MNRAS, 372, 961
Kewley, L. J., Heisler, C. A., & Dopita, M. A. 2001b, ApJS, 132, 37
Kim, D.-C. 1995, PhD thesis, Univ. of Hawaii
Kim, D.-C., & Sanders, D. B. 1998, ApJS, 119, 41
Kim, D.-C., Sanders, D. B., Veilleux, S., Mazzarella, J. M., & Soifer, B. T. 1995, ApJS, 98, 129
Kim, D.-C., Veilleux, S., & Sanders, D. B. 2002, ApJS, 143, 277
Kleinmann, D. E., & Low, F. J. 1970a, ApJ, 159, 165
Kleinmann, D. E., & Low, F. J. 1970b, ApJ, 161, 203
Komossa, S., Burwitz, V., Hasinger, G., Perdehl, P., Kaastra, J. S., & Ikebe, Y. 2003, ApJ, 582, L15
Lípari, S., Terlevich, R., Díaz, R. J., Taniguchi, Y., Zheng, W., Tsvetanov, Z., Carranza, G., & Dottori, H. 2003, MNRAS, 340, 289
Lira, P., Ward, M. J., Zezas, A., & Murray, S. S. 2002, MNRAS, 333, 709
Liu, C. T., & Kennicutt, R. C. 1995, ApJS, 100, 325
Low, F. J., & Kleinmann, D. E. 1968, AJ, 73, 868
Maiolino, R., Ruiz, M., Rieke, G. H., & Keller, L. D. 1995, ApJ, 446, 561
McDowell, J. C., et al. 2003, ApJ, 591, 154
Mihos, J. C., & Hernquist, L. 1994, ApJ, 431, L9
Neugebauer, G., et al. 1984, ApJ, 278, L1
Osterbrock, D. E., & de Robertis, M. M. 1985, PASP, 97, 1129
Pettini, M., & Pagel, B. E. J. 2004, MNRAS, 348, L59
Ptak, A., Heckman, T., Levenson, N. A., Weaver, K., & Strickland, D. 2003, ApJ, 592, 782
Quataert, E. 2001, ASP Conf. Ser. 224, Probing the Physics of Active Galactic Nuclei, ed. B. M. Peterson, R. W. Pogge, & R. S. Polidan (San Francisco, CA: ASP), 71
Rieke, G. H., & Low, F. J. 1972, ApJ, 176, 95
Sanders, D. B. 1999, A&SS, 266, 331
Sanders, D. B., Egami, E., Lipari, S., Mirabel, I. F., & Soifer, B. T. 1995, AJ, 110, 1993
Sanders, D. B., & Mirabel, I. F. 1996, ARA&A, 34, 725
Sanders, D. B., Soifer, B. T., Elias, J. H., Madore, B. F., Matthews, K., Neugebauer, G., & Scoville, N. Z. 1988a, ApJ, 325, 74
Sanders, D. B., Soifer, B. T., Elias, J. H., Neugebauer, G., & Matthews, K. 1988b, ApJ, 328, L35
Soifer, B. T., Boehmer, L., Neugebauer, G., & Sanders, D. B. 1989, AJ, 98, 766
Soifer, B. T., Sanders, D. B., Neugebauer, G., Danielson, G. E., Lonsdale, C. J., Madore, B. F., & Persson, S. E. 1986, ApJ, 303, L41
Soifer, B. T., et al. 1987, ApJ, 320, 238
Strauss, M. A., Huchra, J. P., Davis, M., Yahil, A., Fisher, K. B., & Tonry, J. 1992, ApJS, 83, 29
Sturm, E., et al. 2006, ApJ, 653, L13
Taniguchi, Y., Ikeuchi, S., & Shioya, Y. 1999, ApJ, 514, L9
Tecza, M., Genzel, R., Tacconi, L. J., Anders, S., Tacconi-Garman, L. E., & Thatte, N. 2000, ApJ, 537, 178
Toomre, A., & Toomre, J. 1972, ApJ, 178, 623
Tran, Q. D., et al. 2001, ApJ, 552, 527
Veilleux, S., Kim, D. C., & Sanders, D. B. 1999, ApJ, 522, 113
Veilleux, S., Kim, D. C., & Sanders, D. B. 2002, ApJS, 143, 315
Veilleux, S., Kim, D. C., Sanders, D. B., Mazzarella, J. M., & Soifer, B. T. 1995, ApJS, 98, 171
Veilleux, S., & Osterbrock, D. E. 1987, ApJS, 63, 295
Vorontsov-Velyaminov, B., & Arhipova, V. P. 1968, Morphological Catalogue of Galaxies Volume IV (Moscow: Moscow State Univ.)
Weedman, D. W. 1983, ApJ, 266, 479
Zauderer, B. A., Veilleux, S., & Yee, H. K. C. 2007, ApJ, 659, 1096